Numerical Model of Wave Effects on Permeable Vertical Barriers above the Seabed

By

Gang Yang

B.E., Dalian University of Technology, P.R.China, 1992

M.A.Sc, Dalian University of Technology, P.R.China, 1995

A THESIS SUBMITTED IN PARTIAL FULFILLMENT OF

THE REQUIREMENT FOR THE DEGREE OF

Master of Applied science

in

The Faculty of Graduate Studies

Department of Civil Engineering

We accept this thesis as conforming

to the required standard

THE UNIVERSITY OF BRITISH COLUMBIA

December, 1996

In presenting this thesis in partial fulfillment of the requirements for an advance degree at the University of British Columbia, I agree that the Library shall make it freely available for reference and study. I further agree that permission for extensive copying of this thesis for scholarly purposes may be granted by the head of the department or by his or her representatives. It is understood that copying or publication of this thesis for financial gain shall not be allowed without my written permission.

Department of Civil Engineering,
The University of British Columbia,
2324 Main Mall,
Vancouver, B.C.,
Canada, V6T 1Z4

Date: Dec. 9, 1996

Abstract

This thesis describes a numerical model used to predict the interaction of a regular small amplitude wave train with a thin permeable vertical barrier extending from the water surface to some distance above the seabed. The case of wave interactions with a pair of such barriers is also treated. The approach used is based on an eigenfunction expansion method and utilizes a boundary condition at the barrier surface which accounts for energy dissipation within the barrier. Comparisons of results based on the method have been carried out with those of previous numerical studies for related situations, and close agreement has been obtained in all such cases.

A selection of results based on the method are presented for the transmission, reflection, and energy dissipation coefficients, the wave runup, and the maximum horizontal force on the barrier. These exhibit various features of interest which are discussed.

The numerical model is written in the FORTRAN language. With appropriate input, it can be used to calculate wave interactions with one or two barriers under a wide range of conditions. It is confirmed that the results of the numerical model are consistent for various limiting conditions including those of a solid barrier, a fully transparent barrier, and a barrier extending to the seabed.

Overall, the numerical model is found to provide a reasonably flexible and reliable means of predicting wave effects on thin permeable vertical barriers.

Table of Contents

page

List of Figures

List of Symbols

The following symbols are used in this thesis:

a	=	barrier height, see Fig. 1
A_+	=	see Eqs. 2.63 and 2.64
A_-	=	see Eqs. 2.63 and 2.64
A_{im}	=	unknown coefficients, see Eqs. 2.92-2.94
A_m	=	unknown coefficients, see Eq. 2.39
b	=	barrier thickness, see Fig. 1
b_n	=	see Eqs. 2.45 and 2.47
B_m	=	unknown coefficients, see Eq. 2.40
c	=	wave speed
c_G	=	group speed
C	=	constant, see Eq. 2.2
C_m	=	added mass coefficient
C_{mn}	=	matrix coefficients, see Eqs. 2.45 and 2.46
C_F	=	dimensionless maximum horizontal force coefficient, see Eq. 3.1
C_M	=	dimensionless maximum overturning moment coefficient, see Eq. 3.2
C_R	=	complex reflection coefficient
C_T	=	complex transmission coefficient
d	=	still water depth
E	=	energy flux
f	=	linearized resistance coefficient
f_{mn}	=	see Eq. 2.48
F	=	maximum horizontal wave force
F_s	=	maximum horizontal force of standing waves on a solid barrier, see Eq. 2.79
g	=	gravitational constant

G = complex porous-wall-effect parameter, see Eq. 2.35

G_r = real part of G

G_i = imaginary part of G

h = draft, see Fig. 1

H = wave height

i = $\sqrt{-1}$

K_r = reflection coefficient

K_t = transmission coefficient

K_d = energy dissipation coefficient

k = wave number

m = evanescent mode

M = maximum overturning moment

M_s = maximum overturning moment of standing waves on a solid barrier, see Eq. 2.80

R = wave runup

T = wave period

u = horizontal fluid velocity

$\mathbf{u}$ = spatial velocity vector

$\mathbf{U}$ = general velocity vector

p = spatial pressure

P = general pressure

S = $S'd$, dimensionless complex barrier permeability parameter

S_r = real part of S

S_i = imaginary part of S

S' = G/b, complex barrier permeability parameter

t = time

x = horizontal coordinate, see Figs. 1 and 2

y = horizontal coordinate along the barrier axis

z = vertical coordinate measured upwards from the seabed

Δp = pressure difference across barrier

δ_{1m} = see Eq. 2.139

δ_{2m} = see Eq. 2.142

ε = porosity of barrier

η = wave elevation

λ = half distance between two barriers, see Fig. 2

μ_m = evanescent mode wave numbers for $m \geq 1$

ρ = water density

θ = incident wave angle

Φ = velocity potential, see Eq. 2.1

ϕ = potential function, see Eq. 2.1

ϕ_1 = upwave potential function, see Eqs. 2.39 and 2.92

ϕ_2 = potential function, downwave in case of one barrier, intermediate in case of two barriers, see Eqs. 2.40 and 2.93

ϕ_3 = downwave potential function in case of two barriers, see Eq. 2.94

ϕ_w = incident wave potential function, see Eq. 2.7

ω = wave angular frequency

Ω = dimensionless porous impedance, see Eq. 2.24

The following subscripts are used in this thesis

+ = downwave side (one-barrier case)

- = upwave side (one-barrier case)

0+ = within the barrier at $x = 0$

0- = outside the barrier at $x = 0$

1+ = downwave side of the upwave barrier (two-barrier case)

1- = upwave side of the upwave barrier (two-barrier case)

2+ = downwave side of the downwave barrier (two-barrier case)

2-	=	upwave side of the downwave barrier (two-barrier case)
1	=	fluid region number or the upwave barrier, see Figs. 1 and 2
2	=	fluid region number or the downwave barrier, see Figs. 1 and 2
3	=	fluid region number in case of two barriers, see Fig. 2
b+	=	outside the barrier at x = b
b-	=	within the barrier at x = b
r	=	reflected wave
s	=	standing wave condition for solid barrier
t	=	transmitted wave
w	=	incident wave

Acknowledgments

The author would like to thank his supervisor, Dr. Michael Isaacson, for his guidance throughout the preparation of this thesis. The author would like to express his gratitude to Prof. Dahong Qiu and Prof. Yucheng Li of the Dalian University of Technology for their brilliant teaching and help. Finally, the author is grateful to Mr. Shankar S. Bhat and Mr. Sundaralingam Premasiri for their kind help and encouragement.

Chapter 1 INTRODUCTION

1.1 General

Breakwaters have been used extensively to provide economical protection from waves at many coastal locations. Generally, floating breakwaters are effective only for more modest wave conditions, whereas rubble mound structures are widely used for relatively severe waves. For intermediate wave conditions, floating structures may not be sufficiently effective or robust, whereas rubble mound structures may be expensive and may create environmental problems associated with restricted water circulation.

As an alternative to these two categories of breakwater, breakwaters in the form of thin, rigid vertical barriers have been considered or adopted, especially for marinas and small fishing harbours. A vertical barrier extending from the water surface to some distance above the seabed has the advantages of allowing water circulation, fish passage and sediment transport beneath the breakwater. Such barriers may be impermeable or porous. Parameters such as reflection and transmission coefficients, wave runup, wave force and overturning moment, are very important in the design of such barriers. However, very little is known about wave effects on permeable barriers above the seabed. Thus, wave interactions with thin vertical porous barriers is the subject of this thesis.

The author hopes to extend knowledge on this topic by solving the corresponding linearized boundary value problem in order to obtain various parameters of engineering interest.

1.2 Literature review

Commonly, two approaches are used to predict wave interactions with coastal and offshore structures. One is based on the use of Morison equation, originally proposed by Morison, Johnson, O'Brien and Schaaf (1950). The application of this method carries the implicit

assumption that the structure size is small relative to the wave length so that the incident flow is virtually uniform in the vicinity of the structure. When the structure is relatively large, this is no longer true and an alternative formulation is required. However, since flow separation is now usually unimportant, a theoretical approach may be used in which the corresponding potential flow is treated taking account of boundary conditions introduced by the presence of the structure. The wave forces predicted by solving this diffraction problem to a first approximation were first obtained by MacCamy and Fuchs (1954) for the special case of a large vertical circular cylinder. Within the last few decades, structures of more general shape have been treated by numerical schemes, and this approach generally forms the basis of present prediction methods for large offshore structures.

For certain restricted geometric conditions, the eigenfunction expansion method is widely used as an alternative numerical approach to diffraction problems. Although, problems relating to wave effects on solid barriers and permeable structures have been the subject of numerous theoretical and experimental studies for many years, numerical predictions of wave effects on permeable barriers have been given attention only more recently. In the following sections, a brief review of available theoretical approaches and experimental investigations relating to wave effects on solid and permeable barriers is presented.

1.2.1 Wave effects on impermeable barriers

The prediction of wave effects on fixed, impermeable vertical barriers on the basis of linear wave diffraction theory has been considered by a number of authors.

Ursell (1947) presented an early analytical solution for the transmission coefficient of a barrier extending down from the water surface in deep water waves. For the case of finite depth, Liu and Abbaspour (1982) developed a numerical solution to the linear diffraction problem using a boundary element method. Losada et al. (1992) and Abul-Azm (1993) developed a numerical solution based on the eigenfunction expansion method, and Losada et al. (1993) extended this to the case of random waves.

Wiegel (1960) had earlier proposed a simple prediction of the transmission coefficient based on the hypothesis that the wave energy transmitted past the barrier corresponds to the proportion of incident energy flux associated with the gap beneath the barrier. However, Losada et al. (1992) and Abul-Azm (1993) found notable differences between this approximation and their own accurate solutions.

Recently, Isaacson (1996) developed a variant of an eigenfunction method to provide accurate results over a comprehensive range of conditions, and used this solution to develop simplified expressions for various parameters of engineering interest. These enable such parameters to be estimated with relatively little effort.

1.2.2 Wave effects on permeable structures

Wave interactions with permeable structures have been studied theoretically by a number of authors. These structures include rubble mound structures, wave absorbers, as well as vertical permeable barriers.

Le Méhauté (1971) developed a theory for progressive wave absorbers. The basic principle of the theory is that the energy absorbed by the absorbers is proportional to the area of the plates in contact with water--the plates cause partial reflection of the incident wave due to the sudden narrowing the channel. Experimental results demonstrated qualitatively the validity of this theory.

Sollitt and Cross (1972) derived a theory to predict wave reflection and transmission at a permeable breakwater of rectangular cross section extending from the seabed to the water surface. The theory solves for a damped wave component within the breakwater and matches boundary conditions at the upwave and downwave breakwater faces to predict the reflected and transmitted wave components.

Madsen (1974) derived a simple solution for the reflection and transmission coefficients for a rectangular homogeneous porous structure based on the assumption of

relative long normally incident waves. The solution was based on the linearized form of the governing equations and a linearized form of the flow resistance formula governing the flow within the porous structure.

Macaskill (1978) considered the linearized problem of wave reflection by a thin barrier of arbitrary permeability with the restriction that the flow be two-dimensional. The formulation included the special case of transmission through one or more gaps in an otherwise impermeable barrier. He reduced the general problem to a set of integral equations using standard techniques. A representative range of solutions was obtained numerically for both the finite and infinite depth problems.

Chwang (1982) proposed a porous-wavemaker theory to analyze small-amplitude surface waves on water of finite depth produced by horizontal oscillations of a porous vertical plate. Closed-form solutions were obtained for the surface-wave profile, the hydrodynamic-pressure distribution and the total force on the wavemaker. The influence of a wave-effect parameter and a porous-effect parameter, both dimensionless, on the surface waves and on the hydrodynamic pressure was discussed in detail.

Madsen (1983) presented a theoretical solution for the reflection of linear shallow-water waves from a vertical porous wave absorber on a horizontal bottom. Periodic solutions were matched at the front face of the absorber by assuming continuity of pressure and mass flux. The friction term describing the energy loss inside the absorber was linearized by using Lorentz principle of equivalent work, and, the reflection coefficient was determined as function of parameters describing the incoming waves and the absorber characteristics.

Dalrymple et al. (1990) studied wave reflection and transmission from a porous breakwater using eigenfunction expansions for the water regions in front of the structure, within the porous medium, and behind the structure.

Twu and Lin (1990) investigated a highly effective wave absorber containing a finite number of porous plates with various porous-effect parameters. The relationships of the spacing between the adjacent porous plates as well as the alignment of the plates were analyzed and a formula for evaluating the reflection coefficient was derived. Also, experiments were carried out and the results agree well with the theoretical solutions.

Mallayachari and Sundar (1992) set up a numerical model based on the methodology proposed by Ijima et al. (1976) to determine the reflection characteristics of permeable vertical seawalls and sloping permeable walls. Comparisons of the numerical results with previous analytical results were given.

Losada et al. (1993) used linear theory for water waves impinging obliquely on dissipative multi-layered media to evaluate reflection and transmission coefficients. They examined the case of a periodic medium consisting of alternating layers of upright porous sections and water regions of equal or different thickness.

Yu (1995) studied the diffraction of water waves by thin porous breakwaters extending from the water surface down to the bottom of the seabed based on the linear potential wave theory. A relation for the fluid flow through thin porous structures in addition to the conventional governing equation and boundary conditions for small-amplitude waves in an ideal fluid was derived. A two-dimensional problem with long-crested waves propagating in the normal direction of such an infinite porous wall was first solved and the solution was compared with available experimental data.

Generally, as summarized above, previous theoretical research on permeable barriers are related to barriers or breakwaters extending from the seabed to above the wave surface, whereas little research has been conducted for permeable wave barriers extending from the water surface to above the seabed. Furthermore, past research on permeable wave barriers or breakwaters can be grouped into two categories, depending on the type of flow in the medium. One is based on the assumption of Darcy flow within the medium. In this case, the barriers function as wave absorbers and are often very thin and have a very fine

homogeneous porosity. The other is based on non-Darcy flow within the medium. In this case, the barriers function as rubble mound breakwaters. For the Darcy flow problem, the porous flow velocity is linearly proportional to the pressure difference between the two sides of the porous plate. For the non-Darcy flow problem, the Lorentz principle of equivalent work is often used to represent the velocity field within the barriers.

1.3 Scope of present work

The primary aim of the present investigation is to develop a numerical model to predict the interaction of a regular small-amplitude wave train with a thin permeable vertical barrier extending from the wave surface to some distance above the seabed. The case of wave interactions with a pair of such barriers is also studied.

The approach used is based on an eigenfunction expansion method and linear diffraction theory. Fluid mechanics within a permeable medium is studied and the boundary conditions at the barrier surfaces are thereby developed. Numerical solutions to the problems are presented and the corresponding numerical models are setup.

Comparisons of the numerical results are carried out with those of previous numerical studies for related situations. A selection of numerical results based on the method are presented for the transmission, reflection and energy dissipation coefficients, the wave runup, and the maximum horizontal force on the barrier(s).

It is hoped that this numerical model will help provide designers of coastal barriers with a simple, effective and comprehensive method for wave analysis and the prediction of wave interactions with such barriers.

Chapter 2 THEORETICAL DEVELOPMENT

A definition sketch of a single thin permeable barrier is shown in Fig. 1. It is noted that in practice the barrier is fixed to the seabed by piles, and these are not shown in the figure.

As mentioned earlier, the purpose of the present study is to develop a method for describing regular wave interactions with a thin vertical permeable barrier, extending down from the wave surface to above the seabed (shown as Fig. 1), and then use this to develop expressions for various quantities of engineering interest, including the reflection and transmission coefficients, the wave runup, the wave force and overturning moment.

2.1 Assumptions

In order to simplify the problem, the following assumptions have been made:

i. The fluid is inviscid and incompressible. Thus the flow is irrotational and may be described by a velocity potential which is governed by the Laplace equation.

ii. Linear wave theory is considered suitable for the problem at hand. Thus, the seabed is horizontal and impermeable and wave amplitudes are small.

iii. The barrier is considered to be thin and fixed. Any effect caused by support piles is neglected.

iv. The problem is assumed to be two-dimensional, with the incident waves approaching the barrier normally.

v. There is no overtopping of the waves.

2.2 Governing equations

A regular normally incident small-amplitude wave train of height H and angular frequency ω propagates in water of constant depth d past a thin vertical barrier as shown in Fig. 1. As indicated in the figure, the fluid field is divided into regions 1 and 2, corresponding to the upwave and downwave sides respectively.

A Cartesian coordinate system (x, z) is defined with x measured in the direction of wave propagation from the location of the barrier, and z measured upwards from the seabed. Based on the assumptions mentioned above, the fluid motion can be described by a velocity potential Φ which satisfies the Laplace equation within the fluid region, i.e. $\nabla^2\Phi = 0$. In addition, since the wave height is sufficiently small for linear wave theory to apply, Φ is subject to the usual boundary conditions, linearized where appropriate, at the seabed, free surface and far field. Finally, Φ is subject to appropriate boundary conditions at the structure surface. The velocity potential may thus be expressed, using complex notation, in the form:

$$\Phi(x,z,t) = \mathrm{Re}\left[C\phi(x,z)\exp(-i\omega t)\right] \tag{2.1}$$

where

$$C = -\frac{igH}{2\omega}\,\frac{1}{\cosh(kd)} \tag{2.2}$$

Also, Re[] denotes the real part of the argument, $i = \sqrt{-1}$, t is time, k is the wave number, and g is the gravitational constant.

The potential ϕ in Eq. 2.1 is denoted ϕ_1 and ϕ_2 in regions 1 and 2, corresponding to the upwave and downwave sides of the barrier respectively (see Fig. 1), and different expressions for ϕ_1 and ϕ_2 are developed.

Along the seabed, the vertical velocity of water particle is zero. Thus the boundary conditions at the seabed are

$$\left.\begin{aligned}\frac{\partial\phi_1}{\partial z}&=0\\ \frac{\partial\phi_2}{\partial z}&=0\end{aligned}\right\} \qquad \text{at } z=0 \tag{2.3}$$

Along the wave surface, the free-surface boundary conditions include the kinematic and dynamic boundary conditions, which can be combined into:

$$\left.\begin{aligned}\frac{\partial\phi_1}{\partial z}-\frac{\omega^2}{g}\phi_1&=0\\ \frac{\partial\phi_2}{\partial z}-\frac{\omega^2}{g}\phi_2&=0\end{aligned}\right\} \qquad \text{at } z=d \tag{2.4}$$

where ω is angular frequency of the wave motion.

At large distances from the barrier, ϕ must satisfy a radiation condition, namely

$$\frac{\partial(\phi_1-\phi_w)}{\partial x}=-ik(\phi_1-\phi_w) \qquad \text{at } x=-\infty \tag{2.5}$$

$$\frac{\partial\phi_2}{\partial x}=ik\phi_2 \qquad \text{at } x=+\infty \tag{2.6}$$

where ϕ_w is incident wave potential which is given as:

$$\phi_w=\cosh(kz)\exp(ikx) \tag{2.7}$$

Along the matching boundary within the fluid, x = 0 at $0\le z\le a$, the velocity potential and horizontal velocity are equated:

$$\left.\begin{aligned}\phi_1&=\phi_2\\ \frac{\partial\phi_1}{\partial x}&=\frac{\partial\phi_2}{\partial x}\end{aligned}\right\} \qquad \text{for } x=0\pm \quad 0\le z\le a \tag{2.8}$$

Finally, in order to develop suitable boundary conditions along the barrier surface, the fluid flow within porous media needs to be studied and this is considered in the following section. This is shown to give rise to boundary conditions on the barrier surface as:

$$\frac{\partial \phi_1}{\partial x} = \frac{\partial \phi_2}{\partial x} = -iS'(\phi_2 - \phi_1) \quad \text{for } x = 0\pm \quad a \le z \le d \tag{2.9}$$

where S' is a complex constant (with unit m^{-1}) which depends on the porosity and the thickness of the barrier.

The preceding equations may be collected as follows:

$$\nabla^2 \phi_1 = 0 \qquad \text{in } (-\infty < x < 0; \quad 0 \le z \le d) \tag{2.10}$$

$$\nabla^2 \phi_2 = 0 \qquad \text{in } (0 < x < +\infty; \quad 0 \le z \le d) \tag{2.11}$$

$$\left.\begin{aligned} \frac{\partial \phi_1}{\partial z} &= 0 \\ \frac{\partial \phi_2}{\partial z} &= 0 \end{aligned}\right\} \qquad \text{at } z = 0 \tag{2.12}$$

$$\left.\begin{aligned} \frac{\partial \phi_1}{\partial z} - \frac{\omega^2}{g}\phi_1 &= 0 \\ \frac{\partial \phi_2}{\partial z} - \frac{\omega^2}{g}\phi_2 &= 0 \end{aligned}\right\} \qquad \text{at } z = d \tag{2.13}$$

$$\frac{\partial \phi_1}{\partial x} = \frac{\partial \phi_2}{\partial x} = -iS'(\phi_2 - \phi_1) \quad \text{for } x = 0\pm \quad a \le z \le d \tag{2.14}$$

$$\left.\begin{aligned} \phi_1 &= \phi_2 \\ \frac{\partial \phi_1}{\partial x} &= \frac{\partial \phi_2}{\partial x} \end{aligned}\right\} \qquad \text{for } x = 0\pm \quad 0 \le z \le a \tag{2.15}$$

$$\frac{\partial(\phi_1 - \phi_w)}{\partial x} = -ik(\phi_1 - \phi_w) \quad \text{for } x = -\infty \tag{2.16}$$

$$\frac{\partial \phi_2}{\partial x} = ik\phi_2 \quad \text{for } x = +\infty \tag{2.17}$$

A solution to the above well-posed boundary-value problem is required.

2.3 Flow within barrier

The development of Eq. 2.9 is now considered. The small-amplitude wave motion in an undeformable porous medium may be described by the continuity equation and the convection-neglected Euler equation proposed by Sollitt and Cross (1972) as follows:

$$\nabla \cdot \mathbf{U} = 0 \tag{2.18}$$

$$\frac{\partial \mathbf{U}}{\partial t} = -\frac{\nabla P}{\rho} - f\omega \mathbf{U} - C_m \frac{1-\varepsilon}{\varepsilon} \frac{\partial \mathbf{U}}{\partial t} \tag{2.19}$$

where $\mathbf{U}$ is velocity vector; P is dynamic pressure; ρ is fluid density; ε, f and C_m are the porosity, the linearized resistance coefficient, and the added-mass coefficient of the porous medium respectively.

The last two terms in Eq. 2.19 arise from modeling the porous effect on the fluid motion by two body forces: a linear resistance, which is proportional to the velocity, and an inertia force, which is proportional to the local acceleration. Since the equation arises from a linearization of the friction term which is approximately proportional to velocity squared, it follows that the linearized resistance coefficient f is itself expected to depend on the overall velocity amplitude, and therefore on wave steepness. This aspect is not considered, and here, f is treated as a constant for any given barrier. It is understood that f and C_m, which can only be determined experimentally, depend on the viscosity of the fluid and the porosity of the medium, as well as the geometric shape and the surface properties of the medium pores. Thus f and C_m are treated as constants for any given barrier.

Considering only harmonic solutions, **U** and P can be expressed in the following form:

$$\mathbf{U} = \mathbf{u} \cdot \exp(-i\omega t) \tag{2.20}$$

$$P = p \cdot \exp(-i\omega t) \tag{2.21}$$

where **u** and p are complex amplitudes which are spatial functions only. Substituting Eqs. 2.20 and 2.21 into Eqs. 2.18 and 2.19 yields:

$$\nabla \cdot \mathbf{u} = 0 \tag{2.22}$$

$$\nabla p + \rho\omega\Omega\mathbf{u} = 0 \tag{2.23}$$

where

$$\Omega = f - i\left[1 + C_m \frac{1-\varepsilon}{\varepsilon}\right] \tag{2.24}$$

is a dimensionless porous impedance, whose real and imaginary parts are related respectively to the resistance and the inertial effects of the medium.

For the two-dimensional problem at hand, Eqs. 2.22 and 2.23 can be written as:

$$\frac{\partial u}{\partial x} = 0 \tag{2.25}$$

$$\frac{\partial p}{\partial x} + \rho\omega\Omega u = 0 \tag{2.26}$$

where u is velocity component in the x-direction. Integrating Eq. 2.26 with respect to x over the width b of the barrier, one obtains:

$$u = -\left(p_{b-} - p_{0+}\right)/\left(\rho\omega b\Omega\right) \tag{2.27}$$

where p_{0+} and p_{b-} denote the pressure within the porous medium at $x = 0$ and $x = b$, respectively.

Equation 2.27 states that the x-component of the velocity within the porous medium is proportional to the pressure decrease in the same direction, but with a phase lag. Since Ω has a positive real part and a negative imaginary part, the phase lag is valued between 0 and $\pi/2$. For a medium in which the resistance dominates the inertial effect, the last term of Eq. 2.24 vanishes and $\Omega = f$. The phase lag then tends to zero and, consequently, Eq. 2.27 corresponds to the Darcy's equation:

$$\frac{\partial p}{\partial x} + \rho\omega f u = 0 \tag{2.28}$$

In order to relate the velocity and the pressure within the porous medium with those outside, we consider matching conditions at $x = 0$ and $x = b$. These include the continuity of the mass flux and pressure expressed as:

$$u_{0+} = u_{b-} = \varepsilon u \tag{2.29}$$

$$p_{0-} = p_{0+} \tag{2.30}$$

$$p_{b-} = p_{b+} \tag{2.31}$$

where the subscripts 0+ and 0- denote the values inside and outside the porous medium at $x = 0$, and b- and b+ denote the corresponding values at $x = b$. Substituting Eqs. 2.29, 2.30 and 2.31 into Eq. 2.28, we obtain

$$u_{0-} = -\frac{\varepsilon}{\rho\omega b\Omega}\left(p_{b-} - p_{0+}\right) \qquad \text{at } x = 0- \quad a \le z \le d \tag{2.32}$$

$$u_{b+} = -\frac{\varepsilon}{\rho\omega b\Omega}\left(p_{b-} - p_{0+}\right) \qquad \text{at } x = b+ \quad a \le z \le d \tag{2.33}$$

Without contradicting the small thickness assumption of the porous barrier, the barrier can be treated approximately as a boundary along $x = 0$ and, accordingly, Eqs. 2.32 and 2.33 are applied at $x = 0-$ and $x = 0+$, respectively. Therefore, the boundary condition reduces to:

$$u_{0+} = u_{0-} = -\frac{G}{\rho\omega b}\left(p_{b+} - p_{0-}\right) \qquad \text{at } x = 0\pm \quad a \le z \le d \tag{2.34}$$

where

$$G = \varepsilon/\Omega = G_r + iG_i \tag{2.35}$$

is a complex porous-wall-effect parameter, with G_r being its real part and G_i its imaginary part. It is obvious that G = 0 when either $\varepsilon = 0$ (i.e. solid wall limit) or $\Omega \to \infty$ (both the real and the imaginary parts of Ω tend to infinity). An increase of the value of the real and/or the imaginary part of G corresponds to an increase of the transparency of the wall. For a medium in which the resistance dominates the inertial effect, the porous-wall-effect parameter G becomes real and Eq. 2.34 reduces to that obeying Darcy's law.

Substituting into Eq. 2.34 the following relationships

$$u = \frac{\partial\phi}{\partial x} \tag{2.36}$$

$$p = -\frac{\partial\phi}{\partial t} = i\rho\omega\phi \tag{2.37}$$

the boundary conditions along the surface of the barrier may eventually be expressed as:

$$\frac{\partial\phi_1}{\partial x} = \frac{\partial\phi_2}{\partial x} = -iS'\left(\phi_2 - \phi_1\right) \quad \text{for } x = 0\pm \quad a \le z \le d \tag{2.38}$$

where $S' = G/b$. This corresponds to Eq. 2.9 which has been indicated earlier.

2.4 Solution by eigenfunction expansion method

2.4.1 Eigenfunction expansion method

For the barrier above the seabed, appropriate solutions for the potentials ϕ_1 and ϕ_2 that satisfy Eqs. 2.10-2.13, 2.16, and 2.17 may be written as

$$\phi_1 = \phi_w - \sum_{m=0}^{\infty} A_m \cos(\mu_m z)\exp(\mu_m x) \qquad (x \le 0) \tag{2.39}$$

$$\phi_2 = \phi_w + \sum_{m=0}^{\infty} B_m \cos(\mu_m z)\exp(-\mu_m x) \qquad (x \ge 0) \tag{2.40}$$

where the summation terms represent the scattered wave modes. The variables A_m and B_m are unknown complex coefficients to be determined. In the summation terms,

$$\mu_0 = -ik \tag{2.41}$$

and the remaining values of μ_m are the positive roots of the following equation, taken in ascending order:

$$\mu_m d \tan(\mu_m d) = -\frac{\omega^2 d}{g} \qquad \text{for } m \ge 1 \tag{2.42}$$

Thus, each summation in Eqs. 2.39 and 2.40 represents a superposition of a propagating mode ($m = 0$) and a series of evanescent modes ($m \ge 1$) which decay with distance away from the barrier. Equations 2.39 and 2.40 satisfy all the relevant boundary conditions, except the conditions of pressure continuity along the matching boundary. The boundary condition at the barrier surface are needed to determine the coefficients A_m and B_m.

Through the application of the boundary conditions along the surface of the barrier given by Eq. 2.14, and the matching boundary conditions given by Eq. 2.15, and noting that $\mu_0 = -ik$ and thus $\cos(\mu_0 z) = \cosh(kz)$, it can be shown that $A_m = B_m$ for all m, and

$$\sum_{m=0}^{\infty} A_m \cos(\mu_m z) = 0 \qquad \text{for } 0 \le z \le a \tag{2.43}$$

$$\sum_{m=0}^{\infty} A_m \cos(\mu_m z)(\mu_m - 2iS') = -\mu_0 \cos(\mu_0 z) \qquad \text{for } a \le z \le d \tag{2.44}$$

In previous work based on the eigenfunction expansion method (Losada et al., 1992 and Abul-Azm, 1993), a method involving a least squares fit to the required conditions was used as a basis for estimating A_m. Isaacson (1996) used a simplified integration method to solve for A_m. Here, using Isaacson's method, Eqs. 2.43 and 2.44 are integrated in an appropriate way and then added to develop a suitable matrix equation for A_m. Thus, each equation is first multiplied by $\cos(\mu_n z)$, then integrated with respect to z over the appropriate domain of z (i.e. from z = 0 to a, or from z = a to d, as appropriate), and the resulting two equations are then added. Note that in order to make the units consistent in this addition, Eq. 2.44 is first multiplied by the water depth d. This gives rise to the following matrix equation for A_m:

$$\sum_{m=0}^{\infty} C_{mn} A_m = b_n \qquad \text{for } n = 0,1,\ldots,\infty \tag{2.45}$$

where

$$C_{mn} = f_{mn}(0,a) + (\mu_m d - 2iS) f_{mn}(a,d) \tag{2.46}$$

$$b_n = -\mu_0 d f_{0n}(a,d) \tag{2.47}$$

$$f_{mn}(\alpha,\beta) = \int_{\alpha}^{\beta} \cos(\mu_m z)\cos(\mu_n z)dz$$

$$= \begin{cases} \left[\dfrac{\sin(\mu_- \beta)}{\mu_-} + \dfrac{\sin(\mu_+ \beta)}{\mu_+}\right] - \left[\dfrac{\sin(\mu_- \alpha)}{\mu_-} + \dfrac{\sin(\mu_+ \alpha)}{\mu_+}\right] & (m \neq n) \\ \dfrac{1}{4\mu_m}\left\{\left[2\mu_m \beta + \sin(\mu_m \beta)\right] - \left[2\mu_m \alpha + \sin(\mu_m \alpha)\right]\right\} & (m = n) \end{cases} \tag{2.48}$$

For convenience, the dimensionless parameter $S = S'd$ is used throughout. Also $\mu_- = \mu_m - \mu_n$, and $\mu_+ = \mu_m + \mu_n$.

In a numerical solution to the problem, Eq. 2.45 is truncated to a finite number of terms N, and thus becomes a complex matrix equation of rank N which can be solved for the first

N unknown coefficients A_m. Once these have been obtained, the various quantities of engineering interest may readily be obtained.

2.4.2 Transmission and reflection coefficients

According to linear wave theory, the wave surface elevation is given as:

$$\eta = -\frac{1}{g}\left(\frac{\partial \Phi}{\partial t}\right)_{z=d} \tag{2.49}$$

Substituting Eqs. 2.1, 2.2, 2.39 and 2.40 into the above equation, the complex wave elevation can be obtained as:

$$\eta_1 = \frac{H}{2}\left[\exp(ikx) - \frac{1}{\cosh(kd)}\sum_{m=0}^{\infty} A_m \cos(\mu_m z)\exp(\mu_m x)\right]\exp(-i\omega t) \tag{2.50}$$

$$\eta_2 = \frac{H}{2}\left[\exp(ikx) + \frac{1}{\cosh(kd)}\sum_{m=0}^{\infty} A_m \cos(\mu_m z)\exp(-\mu_m x)\right]\exp(-i\omega t) \tag{2.51}$$

where the subscripts 1 and 2 denote the upwave and downwave sides respectively.

Since the evanescent wave modes ($m \geq 1$) in Eqs. 2.50 and 2.51 decay with distance away from the barrier, only propagating wave modes ($m = 0$) remain at locations far from the barrier. Noting that $\mu_0 = -ik$ and thus $\cos(\mu_0 z) = \cosh(kz)$, the complex transmission and reflection coefficients, denoted here by C_T and C_R respectively, are obtained as:

$$C_T = 1 + A_0 \tag{2.52}$$

$$C_R = -A_0 \tag{2.53}$$

It is obvious that:

$$C_R + C_T = 1 \tag{2.54}$$

For engineering purposes, one usually defines instead real transmission and reflection coefficients, denoted here as K_t and K_r respectively, as the appropriate ratios of wave heights: $K_t = H_t/H$ and $K_r = H_r/H$, where H_t and H_r are the transmitted and reflected wave heights respectively. The relationship between the complex and engineering definitions of transmission and reflection coefficients is simply:

$$K_t = |C_T| = |1 + A_0| \tag{2.55}$$

$$K_r = |C_R| = |A_0| \tag{2.56}$$

2.4.3 Energy balance

An energy loss due to the presence of the barrier should also be considered. The energy flux, which is the average rate of transfer of energy per unit width across a plane of constant x, is defined as

$$E = \overline{\int_0^{d+\eta} \left[p + \frac{1}{2}\rho(u^2 + w^2) + \rho g z \right] u \, dz} \tag{2.57}$$

where an overbar denotes a time average. On the basis of the unsteady Bernoulli equation, and replacing the limit $z = d + \eta$ by $z = d$, since linear theory is used, Eq. 2.57 becomes:

$$E = -\rho \overline{\int_0^d \frac{\partial \Phi}{\partial t} \frac{\partial \Phi}{\partial x} \, dz} \tag{2.58}$$

Recalling the form of Eq. 2.1, E can be expressed as:

$$E = \rho\omega \overline{\int_0^d \mathrm{Re}\left[iC\phi \exp(-i\omega t) \right] \mathrm{Re}\left[C \frac{\partial \phi}{\partial x} \exp(-i\omega t) \right] dx} \tag{2.59}$$

Initially, the energy flux of the incident wave train alone is considered. Thus one takes initially,

$$\phi(x,z) = \phi_w(x,z) = \cosh(kz)\exp(ikx) \tag{2.60}$$

Substituting Eq. 2.60 into 2.59, the energy flux of the incident wave is eventually given by the well-known result (e.g. Sarpkaya and Isaacson, 1981):

$$E_w = \frac{1}{8}\rho g H^2 c_G \tag{2.61}$$

where

$$c_G = \frac{1}{2}\left[1 + \frac{2kd}{\sinh(2kd)}\right] c \tag{2.62}$$

and c is the wave speed.

We consider now the more general case of the wave field at large distances upwave or downwave of the barrier. Far from the barrier, the evanescent wave components are absent and only propagating terms are present. Thus, referring to Eqs. 2.39 and 2.40, in general the velocity potential may be written in the form:

$$\phi(x,z) = \cosh(kz)\left[A_+ \exp(ikx) + A_- \exp(-ikx)\right] \tag{2.63}$$

where A_+ and A_- are the complex dimensionless amplitudes of the waves propagating in the +x and -x directions, respectively.

Substituting Eq. 2.63 into Eq. 2.59, and carrying out the necessary integration, one eventually obtains:

$$E = \frac{1}{8}\rho g H^2 c_G \left(|A_+|^2 - |A_-|^2\right) \tag{2.64}$$

On the upwave side, $A_+ = 1$ and $A_- = -A_0$, and on the downwave side, $A_+ = 1 + A_0$ and $A_- = 0$. Thus one obtains:

$$E_1 = E_w\left(1 - |A_0|^2\right) \tag{2.65}$$

$$E_2 = E_w\left(|1 + A_0|^2\right) \tag{2.66}$$

Consequently the energy flux disipated at the barrier, E_d, is given by

$$E_d = E_1 - E_2 \tag{2.67}$$

Substitute Eqs. 2.65 and 2.66 into Eq. 2.67, finally,

$$E_d = E_w\left(1-\left|A_0\right|^2-\left|1-A_0\right|^2\right) \tag{2.68}$$

An energy loss coefficient can be defined as

$$K_d = \frac{E_d}{E_w} = 1-\left|A_0\right|^2-\left|1-A_0\right|^2 \tag{2.69}$$

From Eqs. 2.55 and 2.56,

$$K_t^{\,2} + K_r^{\,2} = \left|A_0\right|^2+\left|1-A_0\right|^2 \tag{2.70}$$

It is obvious that

$$K_t^{\,2} + K_r^{\,2} + K_d = 1 \tag{2.71}$$

2.4.4 Wave runup

When ϕ_1 and ϕ_2 are used in the representation of Φ (see Eq. 2.1), and x = 0, z = d are taken, then Eq. 2.49 provides the runup on the upwave (subscript -) and downwave (subscript +) sides of the barrier, respectively. The runup can thereby be expressed as

$$R_- = \frac{H}{2}\left|1 - \frac{1}{\cosh(kd)}\sum_{m=0}^{\infty}A_m\cos(\mu_m d)\right| \tag{2.72}$$

$$R_+ = \frac{H}{2}\left|1 + \frac{1}{\cosh(kd)}\sum_{m=0}^{\infty}A_m\cos(\mu_m d)\right| \tag{2.73}$$

2.4.5 Wave loads

On the basis of the linearized, unsteady Bernoulli equation, the hydrodynamic pressure along the upwave and downwave sides of the barrier surface can be expressed respectively as:

$$p_{0-} = -\rho \frac{\partial \Phi_1}{\partial t}\bigg|_{x=-0} \tag{2.74}$$

$$p_{0+} = -\rho \frac{\partial \Phi_2}{\partial t}\bigg|_{x=+0} \tag{2.75}$$

Hence the maximum pressure difference across the barrier, $\Delta p(z)$, is given as:

$$\begin{aligned} \Delta p(z) &= \max\left(p_{0-} - p_{0+}\right) = \max\left[\rho \frac{\partial\left(\Phi_2 - \Phi_1\right)}{\partial t}\right] \\ &= \rho g H \frac{1}{\cosh(kd)}\left|\sum_{m=0}^{\infty} A_m \cos\left(\mu_m z\right)\right| \end{aligned} \tag{2.76}$$

The maximum horizontal force per unit width on the barrier, F, can be obtained by integrating Δp with respect to z. This leads to:

$$F = \rho g H \frac{1}{\cosh(kd)}\left|\sum_{m=0}^{\infty} \frac{A_m\left[\sin\left(\mu_m d\right) - \sin\left(\mu_m a\right)\right]}{\mu_m}\right| \tag{2.77}$$

Likewise, the overturning moment per unit width on the barrier about the seabed, M, can be obtained by an appropriately weighted integration of Δp with respect to z. This leads to:

$$M = \int_a^d \Delta p(z) z dz$$

$$= \rho g H \frac{1}{\cosh(kd)} \left| \sum_{m=0}^{\infty} \frac{A_m \left[\mu_m d \sin(\mu_m d) - \mu_m a \sin(\mu_m a) + \cos(\mu_m d) - \cos(\mu_m a) \right]}{\mu_m^2} \right| \quad (2.78)$$

It is noted that the terms m = 0 in the above equations may readily be expressed directly in terms of real quantities, if required.

2.4.6 Limiting conditions

Various limiting conditions to the preceding solution can be established and are discussed in the following.

Solid barrier ($\varepsilon = 0$)

For a solid barrier $(S_r = S_i = 0)$, various limits to the above solution are known. As $kh \to \infty$ (short wave limit) or as $h/d \to 1$ (full barrier extending to the seabed), the solution should correspond to full reflection on the upwave side, and no wave activity on the downwave side, so that $K_t \to 0$, $K_r \to 1$, $K_d \to 0$, $R_-/H \to 1$, $R_+/H \to 0$, $\Delta p(z) \to \Delta p_s(z)$, $F \to F_s$, and $M \to M_s$; where the subscript s corresponds to the quantities associated with a standing wave train on the upwave side and no wave activity on the downwave side. Expressions for F_s and M_s are easily derived and given respectively as:

$$F_s = \frac{\rho g H}{k} \left[\frac{\sinh(kd) - \sinh(ka)}{\cosh(kd)} \right] \quad (2.79)$$

$$M_s = \frac{1}{2} \frac{\rho g H}{k^2} \left\{ \frac{\left[kd \sinh(kd) - \cosh(kd) \right] - \left[ka \sinh(ka) - \cosh(ka) \right]}{\cosh(kd)} \right\} \quad (2.80)$$

On the other hand, as $kh \to 0$ (long wave limit), or as $h/d \to 0$ (no barrier), the solution should correspond to the undisturbed incident wave field on either side of the barrier, so that $K_t \to 1$, $K_r \to 0$, $K_d \to 0$, $R_-/H \to 1/2$, $R_+/H \to 1/2$, $\Delta p(z) \to 0$, $F \to 0$, and $M \to 0$.

Fully transparent barrier ($\varepsilon = 1$)

A fully transparent barrier $(S_r = +\infty)$ should correspond to the undisturbed incident wave field on either side of the barrier, and so will lead to the same results as above for $kh \to 0$ (the long wave limit), or as $h/d \to 0$ (no barrier). Thus $K_t \to 1$, $K_r \to 0$, $K_d \to 0$, $R_-/H \to 1/2$, $R_+/H \to 1/2$, $\Delta p(z) \to 0$, $F \to 0$, and $M \to 0$.

2.5 Extension to the two-barrier problem

The preceding method can be extended to the two-barrier problem in which an incident wave train interacts with two identical barriers a distance 2λ apart. A definition sketch of the problem is given in Fig. 2. As indicated in the figure, the flow field is now divided into three regions, denoted 1, 2 and 3, corresponding to the regions upwave of the barriers, between the barriers, and downwave of the barriers, respectively.

2.5.1 Governing equations and boundary conditions

The velocity potential Φ within the three fluid regions may be taken as being expressed by the same form as Eq. 2.1. Here, the potential ϕ in Eq. 2.1 is denoted ϕ_1 , ϕ_2 and ϕ_3 in regions 1, 2 and 3. The potentials satisfy the Laplace equation within the fluid region:

$$\nabla^2\phi_1 = 0 \qquad \text{in } (-\infty < x < -\lambda, \quad 0 \le z \le d) \tag{2.81}$$

$$\nabla^2\phi_2 = 0 \qquad \text{in } (-\lambda < x < \lambda, \quad 0 \le z \le d) \tag{2.82}$$

$$\nabla^2\phi_3 = 0 \qquad \text{in } (\lambda < x < +\infty, \quad 0 \le z \le d) \tag{2.83}$$

The boundary conditions along the seabed, free surface, barrier surface, together with the matching conditions and radiation conditions are given respectively by:

$$\left.\begin{aligned}\frac{\partial\phi_1}{\partial z}&=0\\ \frac{\partial\phi_2}{\partial z}&=0\\ \frac{\partial\phi_3}{\partial z}&=0\end{aligned}\right\} \qquad \text{at } z=0 \tag{2.84}$$

$$\left.\begin{aligned}\frac{\partial\phi_1}{\partial z}-\frac{\omega^2}{g}\phi_1&=0\\ \frac{\partial\phi_2}{\partial z}-\frac{\omega^2}{g}\phi_2&=0\\ \frac{\partial\phi_3}{\partial z}-\frac{\omega^2}{g}\phi_3&=0\end{aligned}\right\} \qquad \text{at } z=d \tag{2.85}$$

$$\left.\begin{aligned}\phi_1&=\phi_2\\ \frac{\partial\phi_1}{\partial x}&=\frac{\partial\phi_2}{\partial x}\end{aligned}\right\} \qquad \text{at } \left(x=-\lambda\pm,\quad 0\le z\le a\right) \tag{2.86}$$

$$\left.\begin{aligned}\phi_2&=\phi_3\\ \frac{\partial\phi_2}{\partial x}&=\frac{\partial\phi_3}{\partial x}\end{aligned}\right\} \qquad \text{at } \left(x=+\lambda\pm,\quad 0\le z\le a\right) \tag{2.87}$$

$$\frac{\partial\phi_1}{\partial x}=\frac{\partial\phi_2}{\partial x}=-iS'\left(\phi_2-\phi_1\right) \qquad \text{at } \left(x=-\lambda\pm,\quad a\le z\le d\right) \tag{2.88}$$

$$\frac{\partial\phi_2}{\partial x}=\frac{\partial\phi_3}{\partial x}=-iS'\left(\phi_3-\phi_2\right) \qquad \text{at } \left(x=+\lambda\pm,\quad a\le z\le d\right) \tag{2.89}$$

$$\frac{\partial\left(\phi_1-\phi_w\right)}{\partial x}=-ik\left(\phi_1-\phi_w\right) \qquad \text{for } x=-\infty \tag{2.90}$$

$$\frac{\partial\phi_3}{\partial x}=ik\phi_3 \qquad \text{for } x=+\infty \tag{2.91}$$

2.5.2 Solutions by eigenfunction expansion method

The solutions satisfying the above governing equations and boundary conditions except Eqs. 2.86 - 2.89 can be expressed as:

$$\phi_1 = \phi_w + \sum_{m=0}^{\infty} A_{1m} \cos(\mu_m z) \exp[\mu_m (x+\lambda)] \tag{2.92}$$

$$\phi_2 = \sum_{m=0}^{\infty} A_{2m} \cos(\mu_m z) \exp[-\mu_m (x+\lambda)] + \sum_{m=0}^{\infty} A_{3m} \cos(\mu_m z) \exp[\mu_m (x-\lambda)] \tag{2.93}$$

$$\phi_3 = \sum_{m=0}^{\infty} A_{4m} \cos(\mu_m z) \exp[-\mu_m (x-\lambda)] \tag{2.94}$$

where ϕ_w is incident wave potential which is given by Eq. 2.7. The summation terms in the above equations represent the scattered wave modes. Of these, each summation term represents a superposition of a propagating mode (m = 0) and a series of evanescent modes ($m \geq 1$) which decay with distance away from the barriers. The variables A_{1m}, A_{2m}, A_{3m}, and A_{4m} are unknown complex coefficients to be determined. The eigenvalues μ_m are determined by Eqs. 2.41 and 2.42.

By applying the boundary conditions expressed in Eqs. 2.86 and 2.87, the following equations are obtained for $0 \leq z \leq a$:

$$\sum_{m=0}^{\infty} A_{1m} \cos(\mu_m z) - \sum_{m=0}^{\infty} A_{2m} \cos(\mu_m z) - \sum_{m=0}^{\infty} A_{3m} \cos(\mu_m z) \exp(-2\mu_m \lambda) = -\cos(\mu_0 z) \exp(\mu_0 \lambda) \tag{2.95}$$

$$\sum_{m=0}^{\infty} A_{1m} \mu_m \cos(\mu_m z) + \sum_{m=0}^{\infty} A_{2m} \mu_m \cos(\mu_m z) - \sum_{m=0}^{\infty} A_{3m} \mu_m \cos(\mu_m z) \exp(-2\mu_m \lambda) = \mu_0 \cos(\mu_0 z) \exp(\mu_0 \lambda) \tag{2.96}$$

$$\sum_{m=0}^{\infty} A_{2m} \cos(\mu_m z) \exp(-2\mu_m \lambda) + \sum_{m=0}^{\infty} A_{3m} \cos(\mu_m z) - \sum_{m=0}^{\infty} A_{4m} \cos(\mu_m z) = 0 \tag{2.97}$$

$$\sum_{m=0}^{\infty} A_{2m}\mu_m \cos(\mu_m z)\exp(-2\mu_m\lambda) - \sum_{m=0}^{\infty} A_{3m}\mu_m \cos(\mu_m z) - \sum_{m=0}^{\infty} A_{4m}\mu_m \cos(\mu_m z) = 0 \tag{2.98}$$

By applying the boundary conditions along the barrier's surface (expressed as Eqs. 2.88 and 2.89), the following equations are obtained for $a \le z \le d$:

$$\sum_{m=0}^{\infty} A_{1m} \cos(\mu_m z)(\mu_m - iS') + iS' \sum_{m=0}^{\infty} A_{2m} \cos(\mu_m z) + iS' \sum_{m=0}^{\infty} A_{3m} \cos(\mu_m z)\exp(-2\mu_m\lambda) = (\mu_0 + iS')\cos(\mu_0 z)\exp(\mu_0\lambda) \tag{2.99}$$

$$iS' \sum_{m=0}^{\infty} A_{1m} \cos(\mu_m z) + \sum_{m=0}^{\infty} A_{2m} \cos(\mu_m z)(\mu_m - iS') - \sum_{m=0}^{\infty} A_{3m} \cos(\mu_m z)\exp(-2\mu_m\lambda)(\mu_m + iS') = -iS'\cos(\mu_0 z)\exp(\mu_0\lambda) \tag{2.100}$$

$$\sum_{m=0}^{\infty} A_{2m} \cos(\mu_m z)\exp(-2\mu_m\lambda)(\mu_m + iS') - \sum_{m=0}^{\infty} A_{3m} \cos(\mu_m z)(\mu_m - iS') - iS' \sum_{m=0}^{\infty} A_{4m} \cos(\mu_m z) = 0 \tag{2.101}$$

$$iS' \sum_{m=0}^{\infty} A_{2m} \cos(\mu_m z)\exp(-2\mu_m\lambda) + iS' \sum_{m=0}^{\infty} A_{3m} \cos(\mu_m z) + \sum_{m=0}^{\infty} A_{4m} \cos(\mu_m z)(\mu_m - iS') = 0 \tag{2.102}$$

As an extension to the solution for the single barrier problem, Eqs. 2.95 and 2.99, 2.96 and 2.100, 2.97 and 2.101, 2.98 and 2.102 are integrated with respect to z over 0 to a or over a to d as appropriate, and each pair of resulting equations is then added to obtain four sets of equations for A_{im}. (Some equations are first multiplied by d to make the units consistent.) These are:

$$\begin{aligned}
&\sum_{m=0}^{\infty} A_{1m}\left[f_{mn}(0,a)+(\mu_m d-iS)f_{mn}(a,d)\right] \\
&\quad+\sum_{m=0}^{\infty} A_{2m}\left[-f_{mn}(0,a)+iSf_{mn}(a,d)\right] \\
&\quad+\sum_{m=0}^{\infty} A_{3m}\exp(-2\mu_m\lambda)\left[-f_{mn}(0,a)+iSf_{mn}(a,d)\right] \\
&\quad=-\exp(\mu_0\lambda)f_{0n}(0,a)+(\mu_0 d+iS)\exp(\mu_0\lambda)f_{0n}(a,d)
\end{aligned} \tag{2.103}$$

$$\begin{aligned}
&\sum_{m=0}^{\infty} A_{1m}\left[\mu_m df_{mn}(0,a)+iSf_{mn}(a,d)\right] \\
&\quad+\sum_{m=0}^{\infty} A_{2m}\left[\mu_m df_{mn}(0,a)+(\mu_m d-iS)f_{mn}(a,d)\right] \\
&\quad+\sum_{m=0}^{\infty} A_{3m}\exp(-2\mu_m\lambda)\left[-\mu_m df_{mn}(0,a)-(\mu_m d+iS)f_{mn}(a,d)\right] \\
&\quad=\mu_0 d\exp(\mu_0\lambda)f_{0n}(0,a)-iS\exp(\mu_0\lambda)f_{0n}(a,d)
\end{aligned} \tag{2.104}$$

$$\begin{aligned}
&\sum_{m=0}^{\infty} A_{2m}\exp(-2\mu_m\lambda)\left[f_{mn}(0,a)+(\mu_m d+iS)f_{mn}(a,d)\right] \\
&\quad+\sum_{m=0}^{\infty} A_{3m}\left[f_{mn}(0,a)-(\mu_m d-iS)f_{mn}(a,d)\right] \\
&\quad+\sum_{m=0}^{\infty} A_{4m}\left[-f_{mn}(0,a)-iSf_{mn}(a,d)\right]=0
\end{aligned} \tag{2.105}$$

$$\begin{aligned}
&\sum_{m=0}^{\infty} A_{2m}\exp(-2\mu_m\lambda)\left[\mu_m df_{mn}(0,a)+iSf_{mn}(a,d)\right] \\
&\quad+\sum_{m=0}^{\infty} A_{3m}\left[-\mu_m df_{mn}(0,a)+iSf_{mn}(a,d)\right] \\
&\quad+\sum_{m=0}^{\infty} A_{4m}\left[-\mu_m df_{mn}(0,a)+(\mu_m d-iS)f_{mn}(a,d)\right]=0
\end{aligned} \tag{2.106}$$

where the function $f_{mn}()$ is defined by Eq. 2.48.

Equations 2.101 - 2.104 can be expressed as the following matrix equation for A_{1m}, A_{2m}, A_{3m} and A_{4m}:

$$\begin{bmatrix} \sum_{m=0}^{\infty} C_{11}^{(mn)} & \sum_{m=0}^{\infty} C_{12}^{(mn)} & \sum_{m=0}^{\infty} C_{13}^{(mn)} & \sum_{m=0}^{\infty} C_{14}^{(mn)} \\ \sum_{m=0}^{\infty} C_{21}^{(mn)} & \sum_{m=0}^{\infty} C_{22}^{(mn)} & \sum_{m=0}^{\infty} C_{23}^{(mn)} & \sum_{m=0}^{\infty} C_{24}^{(mn)} \\ \sum_{m=0}^{\infty} C_{31}^{(mn)} & \sum_{m=0}^{\infty} C_{32}^{(mn)} & \sum_{m=0}^{\infty} C_{33}^{(mn)} & \sum_{m=0}^{\infty} C_{34}^{(mn)} \\ \sum_{m=0}^{\infty} C_{41}^{(mn)} & \sum_{m=0}^{\infty} C_{42}^{(mn)} & \sum_{m=0}^{\infty} C_{43}^{(mn)} & \sum_{m=0}^{\infty} C_{44}^{(mn)} \end{bmatrix} \begin{Bmatrix} A_{1m} \\ A_{2m} \\ A_{3m} \\ A_{4m} \end{Bmatrix} = \begin{Bmatrix} b_{1n} \\ b_{2n} \\ b_{3n} \\ b_{4n} \end{Bmatrix} \tag{2.107}$$

where

$$C_{11}^{(mn)} = f_{mn}(0,a) + (\mu_m d - iS) f_{mn}(a,d) \tag{2.108}$$

$$C_{12}^{(mn)} = -f_{mn}(0,a) + iSf_{mn}(a,d) \tag{2.109}$$

$$C_{13}^{(mn)} = \exp(-2\mu_m \lambda)\left[-f_{mn}(0,a) + iSf_{mn}(a,d)\right] \tag{2.110}$$

$$C_{21}^{(mn)} = \mu_m d f_{mn}(0,a) + iSf_{mn}(a,d) \tag{2.111}$$

$$C_{22}^{(mn)} = \mu_m d f_{mn}(0,a) + (\mu_m d - iS) f_{mn}(a,d) \tag{2.112}$$

$$C_{23}^{(mn)} = \exp(-2\mu_m \lambda)\left[-\mu_m d f_{mn}(0,a) - (\mu_m d + iS) f_{mn}(a,d)\right] \tag{2.113}$$

$$C_{32}^{(mn)} = \exp(-2\mu_m \lambda)\left[f_{mn}(0,a) + (\mu_m d + iS) f_{mn}(a,d)\right] \tag{2.114}$$

$$C_{33}^{(mn)} = f_{mn}(0,a) - (\mu_m d - iS) f_{mn}(a,d) \tag{2.115}$$

$$C_{34}^{(mn)} = -f_{mn}(0,a) - iSf_{mn}(a,d) \tag{2.116}$$

$$C_{42}^{(mn)} = \exp(-2\mu_m \lambda)\left[\mu_m d f_{mn}(0,a) + iSf_{mn}(a,d)\right] \tag{2.117}$$

$$C_{43}^{(mn)} = -\mu_m d f_{mn}(0,a) + iSf_{mn}(a,d) \tag{2.118}$$

$$C_{44}^{(mn)} = -\mu_m d f_{mn}(0,a) + (\mu_m d - iS) f_{mn}(a,d) \tag{2.119}$$

$$C_{14}^{(mn)} = C_{24}^{(mn)} = C_{31}^{(mn)} = C_{41}^{(mn)} = 0 \tag{2.120}$$

$$b_{1n} = \exp(\mu_0\lambda)\left[-f_{0n}(0,a)+(\mu_0 d+iS)f_{0n}(a,d)\right] \tag{2.121}$$

$$b_{2n} = \exp(\mu_0\lambda)\left[\mu_0 d f_{0n}(0,a)-iSf_{0n}(a,d)\right] \tag{2.122}$$

$$b_{3n} = b_{4n} = 0 \tag{2.123}$$

In a numerical solution to the problem, Eq. 2.107 is truncated to a finite number of terms N, and thus becomes a complex matrix equation of rank 4N which can be solved for the first N unknown values of each set of coefficients A_{1m}, A_{2m}, A_{3m} and A_{4m}. Once these have been calculated, the various quantities of engineering interest may readily be obtained.

The transmission and reflection coefficients are given in terms of A_{1m} and A_{4m} by:

$$K_t = |A_{40}| \tag{2.124}$$

$$K_r = |A_{10}| \tag{2.125}$$

Considering energy conservation, at large distances from the two barriers, $x-\lambda$ and $x+\lambda$ are equivalent to x. Therefore, Eq. 2.63 can still be used to express the upwave and downwave wave potentials ϕ_1 and ϕ_3. Here, on the upwave side, $A_+ = 1$, $A_- = A_{10}$, and on the downwave side, $A_- = A_{40}$, $A_- = 0$. Substituting these values into Eq. 2.64, the energy flux on the upwave and downwave sides, E_1 and E_3 respectively, can be expressed as:

$$E_1 = E_w\left(1-|A_{10}|^2\right) \tag{2.126}$$

$$E_3 = E_w|A_{40}|^2 \tag{2.127}$$

Consequently the energy flux dissipated at the barriers, E_d, is given by

$$E_d = E_1 - E_3 = E_w\left(1-|A_{10}|^2-|A_{40}|^2\right) \tag{2.128}$$

Therefore the energy dissipation coefficient can be obtained as:

$$K_d = \frac{E_d}{E_w} = 1 - |A_{10}|^2 - |A_{40}|^2 \tag{2.129}$$

From considerations of energy conservation, substituting Eqs. 2.124 and 2.125 into Eq. 2.129, these are related to the energy dissipation coefficient K_d:

$$K_r^2 + K_t^2 + K_d = 1 \tag{2.130}$$

The wave runup on both sides of each barrier can be obtained as:

$$R_{1-} = \frac{H}{2}\left|\exp(\mu_0\lambda) + \frac{1}{\cosh(kd)}\sum_{m=0}^{\infty} A_{1m}\cos(\mu_m d)\right| \tag{2.131}$$

$$R_{1+} = \frac{H}{2}\left|\frac{1}{\cosh(kd)}\left[\sum_{m=0}^{\infty} A_{2m}\cos(\mu_m d) + \sum_{m=0}^{\infty} A_{3m}\cos(\mu_m d)\exp(-2\mu_m\lambda)\right]\right| \tag{2.132}$$

$$R_{2-} = \frac{H}{2}\left|\frac{1}{\cosh(kd)}\left[\sum_{m=0}^{\infty} A_{2m}\cos(\mu_m d)\exp(-2\mu_m\lambda) + \sum_{m=0}^{\infty} A_{3m}\cos(\mu_m d)\right]\right| \tag{2.133}$$

$$R_{2+} = \frac{H}{2}\left|\frac{1}{\cosh(kd)}\sum_{m=0}^{\infty} A_{4m}\cos(\mu_m d)\right| \tag{2.134}$$

where R_{1-} and R_{1+} denote the wave runup on the upwave side and downwave side of the barrier 1, and R_{2-} and R_{2+} denote the wave runup on the upwave side and downwave side of the barrier 2, respectively.

The maximum pressure difference across each barrier can be obtained by:

$$\Delta p_1(z) = \max\left(p_{-\lambda-} - p_{-\lambda+}\right) = \max\left[\rho\frac{\partial\left(\Phi_2 - \Phi_1\right)}{\partial t}\right]_{x=-\lambda}$$

$$= \frac{\rho g H}{2\cosh(kd)}\left|\sum_{m-0}^{\infty} A_{1m}\cos\left(\mu_m z\right) - \sum_{m-0}^{\infty} A_{2m}\cos\left(\mu_m z\right) - \right. \tag{2.135}$$

$$\left. \sum_{m-0}^{\infty} A_{3m}\cos\left(\mu_m z\right)\exp\left(-2\mu_m\lambda\right) + \cos\left(\mu_0 z\right)\exp\left(\mu_0\lambda\right)\right|$$

$$\Delta p_2(z) = \max\left(p_{\lambda-} - p_{\lambda+}\right) = \max\left[\rho\frac{\partial\left(\Phi_3 - \Phi_2\right)}{\partial t}\right]_{x=\lambda}$$

$$= \frac{\rho g H}{2\cosh(kd)}\left|\sum_{m-0}^{\infty} A_{2m}\cos\left(\mu_m z\right)\exp\left(-2\mu_m\lambda\right) + \right. \tag{2.136}$$

$$\left. \sum_{m-0}^{\infty} A_{3m}\cos\left(\mu_m z\right) - \sum_{m-0}^{\infty} A_{4m}\cos\left(\mu_m z\right)\right|$$

Integrating Eqs. 2.135 and 2.136 with respect to z, result in the maximum horizontal force per unit length on each barrier:

$$F_1 = \frac{\rho g H}{2\cosh(kd)}\left|\sum_{m=0}^{\infty} A_{1m}\delta_{1m} - \sum_{m=0}^{\infty} A_{2m}\delta_{1m}\right.$$

$$\left. - \sum_{m=0}^{\infty} A_{3m}\delta_{1m}\exp\left(-2\mu_m\lambda\right) + \delta_{10}\exp\left(\mu_0\lambda\right)\right| \tag{2.137}$$

$$F_2 = \frac{\rho g H}{2\cosh(kd)}\left|\sum_{m=0}^{\infty} A_{2m}\delta_{1m}\exp\left(-2\mu_m\lambda\right) + \sum_{m=0}^{\infty} A_{3m}\delta_{1m} - \sum_{m=0}^{\infty} A_{4m}\delta_{1m}\right| \tag{2.138}$$

where

$$\delta_{1m} = \frac{\sin\left(\mu_m d\right) - \sin\left(\mu_m a\right)}{\mu_m} \tag{2.139}$$

The overturning moment per unit width on each barrier about the seabed can be obtained as:

$$M_1 = \frac{\rho g H}{2\cosh(kd)}\left|\sum_{m=0}^{\infty} A_{1m}\delta_{2m} - \sum_{m=0}^{\infty} A_{2m}\delta_{2m} - \sum_{m=0}^{\infty} A_{3m}\delta_{2m}\exp(-2\mu_m\lambda) + \delta_{20}\exp(\mu_0\lambda)\right| \tag{2.140}$$

$$M_2 = \frac{\rho g H}{2\cosh(kd)}\left|\sum_{m=0}^{\infty} A_{2m}\delta_{2m}\exp(-2\mu_m\lambda) + \sum_{m=0}^{\infty} A_{3m}\delta_{2m} - \sum_{m=0}^{\infty} A_{4m}\delta_{2m}\right| \tag{2.141}$$

where

$$\delta_{2m} = \frac{\mu_m d\sin(\mu_m d) - \mu_m a\sin(\mu_m a) + \cos(\mu_m d) - \cos(\mu_m a)}{\mu_m^2} \tag{2.142}$$

Chapter 3 DEVELOPMENT OF NUMERICAL MODEL

3.1 General

Based on the theoretical analysis outlined in the preceding chapter, a numerical model written in the FORTRAN language has been developed. The objective of setting up the numerical model is to obtain various quantities of engineering interest, such as the transmission and reflection coefficients, the dimensionless wave runup, and the wave forces acting on the barriers. As mentioned in Chapter 2, all these quantities depend on the coefficients A_m (one-barrier problem) or the coefficients A_{1m}, A_{2m}, A_{3m} and A_{4m} (two-barrier problem). Thus the task becomes one of calculating the various coefficients C_{mn} and solving the matrix equations given by Eq. 2.45 (one-barrier problem) and Eq. 2.107 (two-barrier problem). Once these coefficients are obtained, the required quantities can readily be calculated in the manner indicated.

3.2 Parameter selection

Before setting up the numerical model, it is appropriate to consider initially the selection of suitable input and output parameters. The input parameters include the incident wave conditions (wave height, wave period, water depth), barrier conditions (the draft h, the permeability parameter S'). The output parameters include the transmission and reflection coefficients, the wave runup, the wave forces and the overturning moments.

In presenting results of the numerical model, it is useful to carry out a dimensional analysis. Bearing in mind that the independent parameters may be considered as H, d, h, k and S' (also λ for the two-barrier problem), a dimensional analysis indicates that the independent parameters can be selected as, for example, kh (or kd), h/d, λ/d, and S ($S = S'd$). It is unnecessary to specify the wave height H since the dimensionless output parameters are obtained in dimensionless form which are themselves independent of H. As

indicated in Chapter 2, the permeability parameter S' can be only obtained by experiments, thus S is treated as an input value in the numerical model.

The output parameters are all expressed in dimensionless form. These parameters include transmission and reflection coefficients, wave runup coefficients, wave force coefficients and overturning moment coefficients. The wave runup coefficients are defined as R/H, and the dimensionless force coefficients and the overturning moment coefficients are defined as:

$$C_F = \frac{F}{\rho g H d} \tag{3.1}$$

$$C_M = \frac{M}{\rho g H d^2} \tag{3.2}$$

Chapter 4 RESULTS AND DISCUSSION

A range of numerical results have been obtained in order to examine the validity of the numerical model and to provide predictions for practical situations. Also, comparisons with previous predictions have been carried out.

4.1 One-barrier problem

Previous numerical results for wave interactions with a permeable vertical barrier fixed above the seabed appear not to be available. Thus, in order to examine the effectiveness of the numerical model, comparisons are made with previous predictions for the following two limiting cases: a solid barrier above the seabed (Abul-Azm, 1993, Losada et al., 1992, and Isaacson, 1996), and a permeable barrier extending down to the seabed (Yu, 1995). Subsequently, results for a single permeable barrier above the seabed are presented and discussed. These provide various quantities of engineering interest as functions of the dimensionless wave frequency kh, the relative penetration of the barrier h/d, and the dimensionless permeability parameter S.

4.1.1 Comparisons with previous predictions

For a solid barrier above the seabed (S = 0), the problem becomes exactly that treated previously by several authors, including Losada et al. (1992), Abul-Azm (1993) and Isaacson (1996). For this limiting case, the present numerical model coincides exactly with that of Isaacson (1996), and is slightly different from that used by Abul-Azm and Losada et al. in that the coefficients A_m are obtained here by a simplified integration method rather than a least squares method. The present numerical results have been compared with those of previous studies for a wide range of conditions, and in all cases show very close agreement. Differences among the results are not distinguishable on ordinary plots and hence are not shown here.

For a permeable barrier extending from the free surface down to the bottom of the seabed ($h/d = 1$), the problem becomes exactly that solved by Yu (1995). The transmission and reflection coefficients as functions of the permeability parameter S have been calculated by the present method for a range of relative water depths kd and compared with the results given by Yu. Once more, the agreement has been found to be very close.

4.1.2 Transmission and reflection coefficients

Figure 3 shows the transmission coefficient K_t and the reflection coefficient K_r as functions of S for the case $kh = 0.5$ and $h/d = 0.5$. The results are shown as contours of each parameter plotted in the complex S plane. S_r and S_i denote the real and imaginary parts of S respectively. The waviness in some of the contours is due to the contour fitting program that was used. The results for $S = 0$, for which $K_t = 0.93$ and $K_r = 0.37$, correspond to the case of an impermeable barrier. The results along the abscissa (S_r) correspond to the Darcy flow assumption, with increasing S_r corresponding to increasing porosity, decreasing friction coefficient, and/or decreasing barrier width (see Eqs. 2.24 and 2.35). This figure shows that K_r decreases with increasing values of both the real and imaginary components of S; that K_t varies quite strongly with S_r, initially decreasing and then increasing as the value of S_r increases; and that K_t varies quite weakly with S_i.

Figures 4 and 5 show K_t and K_r as functions of kh for the case $h/d = 0.5$ and for various values of S. The selected values of S correspond to an impermeable barrier ($S = 0$), the Darcy flow assumption with a smaller porosity ($S = 0.5$) and a larger porosity ($S = 2.0$), and two cases when both frictional and inertial effects are equally important ($S = 0.5 + 0.5i$, $S = 2.0 + 2.0i$). Figure 4 shows how K_t decreases as kh increases. The case of an impermeable barrier ($S = 0$) is seen to give a lower transmission coefficient than a porous barrier, as expected, while the case of the more porous barrier ($S = 2.0 + 2.0i$) generally gives the highest transmission coefficient. The two cases $S = 2.0$ and $S = 2.0 + 2.0i$ indicate that S_i has a relatively small effect on K_t and K_r in comparison to S_r. The opposite trends for the reflection coefficient are indicated in Fig. 5.

Figures 6 and 7 show K_t and K_r as functions of h/d for kd = 1.0 and for various values of S. The figures indicate that K_t decreases as h/d increases, and K_r increases as h/d increases, as expected. It is noted that the differences of K_t and K_r among the barriers with different S values become more significant as h/d increases. It is also noted that for a solid barrier (S = 0), as $kh \to \infty$ (short wave limit) or as $h/d \to 1$ (full barrier extending to the seabed), the numerical results correspond to the expected limit of full reflection on the upwave side, and no wave activity on the downwave side: $K_t \to 0$, $K_r \to 1$.

4.1.3 Energy dissipation coefficient

Figure 8 shows the energy dissipation coefficient K_d as contours in the complex S plane for the case $kh = 0.5$, $h/d = 0.5$ corresponding to Fig. 3. Figure 9 shows K_d as a function of kh for $h/d = 0.5$ and for various values of S. As indicated in these figures, K_d increases initially and then decreases as S_r increases, and decreases quite weakly with S_i. It is seen that the energy dissipation coefficient reaches a maximum for a certain value of S under a specified wave condition, or under a certain wave condition for a specified barrier. For example, in Fig. 8, when $h/d = 0.5$ and $kh = 0.5$, a barrier with approximately S = 0.7 gives rise to a maximum energy dissipation coefficient $K_d \approx 0.26$, and as shown in Fig. 9, when S = 0.5, a maximum $K_d \approx 0.45$ is reached when kh = 1.0.

Figure 10 shows the energy dissipation coefficient as a function of h/d for kd = 1.0 and for various values of S. This figure indicates how K_d increases as h/d increases. A solid barrier does not give rise to any energy dissipation so that a solid line cannot be observed.

4.1.4 Wave loads

Figure 11 shows the force coefficient C_F as contours in the complex S plane for the case $h/d = 0.5$, $kh = 0.5$; Fig. 12 shows C_F as a function of kh for $h/d = 0.5$ and for various values of S; and Fig. 13 shows C_F as a function of h/d for kd = 1.0 and for various values of S. These figures indicate that the wave force coefficient first increases with a decrease

of S_i or S_r, and reaches the maximum as S = 0; that the wave force coefficient increases sharply and then decreases more gradually as kh increases giving a peak value under certain wave conditions; and that the wave force coefficient increases as h/d increases, as expected.

Figures 14, 15 and 16 show the overturning moment coefficient C_M as a function of S, kh, and h/d respectively for various conditions. These figures indicate exactly the same trends as those of the force coefficient C_F.

4.1.5 Wave runup

Figure 17 shows the wave runup coefficients for both sides of the barrier, R_-/H and R_+/H, as contours in the complex S plane for the case $h/d = 0.5$, $kh = 0.5$. The wave runup on the upwave side of the barrier (shown as solid lines) initially increases, then decreases as S_r increases. The opposite trend is seen for the wave runup on the downwave side of the barrier (shown as broken lines). The wave runup on both sides vary slowly as S_i increases. These phenomena coincide with that of the wave energy dissipation coefficient.

The wave runup coefficients on the upwave side and the downwave side as functions of kh for $h/d = 0.5$ and for various values of S are shown in Figs. 18 and 19. These figures show that, for a porous barrier, the wave runup on the upwave side increases as kh increases, and the magnitude ranges from H/2 to H. On the other hand, the wave runup on the downwave side decreases from H/2 to a small value (0 for a solid barrier) as kh increases.

The wave runup coefficients on the upwave side and the downwave side as functions of h/d for $kd = 1.0$ and for various values of S are shown in Figs. 20 and 21. It is seen that the wave runup on the upwave side increases as h/d increases, and reaches a constant value for a more porous barrier. The wave runup on the downwave side, on the other hand, decreases as h/d increases, and also reaches a constant value for more porous barrier.

It is noticed that for a solid barrier (S = 0), as $kh \to \infty$ (short wave limit) or as $h/d \to 1$ (full barrier extending to the seabed), the numerical results correspond to full reflection on the upwave side, and no wave activity on the downwave side, so that, $R_-/H \to 1$, $R_+/H \to 0$.

4.2 Two-barrier problem

Previous results for wave interactions with two permeable vertical barriers fixed above the seabed appear not to be available. Thus no comparison can be made to examine the effectiveness of the numerical model for two-barrier problem. However, for some limiting conditions, some results are evident and can be examined by the numerical model. Bearing in mind the difficulty of checking the numerical model, it is nevertheless useful to examine the numerical prediction of wave effects on two permeable vertical barriers.

4.2.1 Transmission and reflection coefficients

Figure 22 shows the transmission and reflection coefficients as contours in the complex S plane for the case $h/d = 0.5$, $kh = 0.5$, $\lambda/d = 1.0$. It is seen that, similar to the one-barrier case, K_r decreases with increasing values of both the real and imaginary components of S; K_t varies quite strongly with S_r, initially decreasing and then increasing as the value of S_r increases; K_t varies quite weakly with S_i. It is noted that both the values of K_t and K_r are smaller than the corresponding values for the one-barrier case.

Figures 23 and 24 show the transmission and reflection coefficients as functions of kh for $h/d = 0.5$, $\lambda/d = 1.0$ and for various values of S. Generally, K_t decreases and K_r increases as kh increases. However, under certain wave conditions, phenomena of resonance occur, where K_t increases sharply, and K_r decreases sharply. The figures show that for solid barriers there are two points of significant resonance occurring at $kh = 0.907$ and $kh = 1.585$. For permeable barriers, additional phenomena of resonance can be seen. Thus K_t and K_r vary periodically with kh.

Figures 25 and 26 show the transmission and reflection coefficients as functions of λ/d for $h/d = 0.5$, $kd = 1.0$ and for various values of S. It is seen that K_t and K_r increase and decrease periodically as λ/d increases, and the magnitudes of changing values of K_t and K_r decrease as S increases. It is found that the peak (or trough) values of K_t and/or K_r repeatedly occur when the distance between the two barriers is increase by nL/4 (n=1,2,...), where L is the wave length. Since the phase angles are dependent on the wave conditions (wave period, water depth) and barrier conditions (barrier length under the water, the width, the porosity parameter), the points of λ/d at which the peak (or trough) values of K_t (or K_r) occur are different for different values of S as $h/d = 0.5$ and $kd = 1.0$, but still can be calculated.

4.2.2 Energy dissipation coefficient

The energy dissipation coefficient K_d as contours in the complex S plane for the case $h/d = 0.5$, $kh = 0.5$, $\lambda/d = 1.0$ is shown in Fig. 27. As indicated in the figure, K_d increases initially and then decreases as S_r increases, and decreases quite weakly with S_i. The maximum energy dissipation coefficient occurs for a certain value of S under a specified wave condition, or under a certain wave condition for a specified barrier. As shown in Fig. 27, when $h/d = 0.5$, $kh = 0.5$ and $\lambda/d = 1.0$, the barriers with approximately S = 0.7 give rise to a maximum wave energy dissipation coefficient $K_d \approx 0.52$. Compared with the one-barrier case shown in Fig. 8 (a maximum wave energy dissipation coefficient $K_d \approx 0.26$), it's seen that more energy is dissipated.

Figure 28 shows the energy dissipation coefficient as a function of kh for $h/d = 0.5$, $\lambda/d = 1.0$ and for various values of S. As shown in the figure, generally K_d increases initially and then decreases as kh increases, but varies periodically as kh changes in small ranges. The energy dissipation coefficient for solid barriers appears to be zero, as expected. For permeable barriers, the K_d value reaches its maximum under certain wave conditions.

Figure 29 shows the energy dissipation coefficient as a function of λ/d for $h/d = 0.5$, $kd = 1.0$ and for various values of S. This figure indicates that, K_d varies periodically as the distance between the two barriers increases. The magnitudes of changing values of K_d decrease as S increases. It is also found that the maximum (or minimum) values of K_d repeatedly occur as the distance between the two barriers is increased by nL/4 (n = 1,2,...), where L is the wave length.

4.2.3 Wave forces

Figures 30 and 31 show the wave force coefficients C_F of the upwave barrier and the downwave barrier as contours in the complex S plane for $h/d = 0.5$, $kh = 0.5$ and $\lambda/d = 1.0$. The force coefficients C_F of the upwave barrier and the downwave barrier as functions of kh are shown in Figs. 32 and 33 for $h/d = 0.5$, $\lambda/d = 1.0$ and for various values of S. Figures 34 and 35 show the C_F values for the upwave and the downwave barriers as a function of λ/d for $h/d = 0.5$, $kd = 1.0$ and for various values of S. The figures indicate that the wave forces acting on the barriers decrease as S_r and/or S_i increases. The wave force acting on the downwave side barrier is smaller than that acting on the upwave barrier. Some resonance phenomena occur under certain wave conditions, which give rise to relatively high or low values of C_F. The C_F values of both barriers vary periodically as the distance between the barriers increases by nL/4 (n=1,2,...), where L is the wave length. As the barriers are more porous (S increases), the forces acting on the barriers become more stable and vary slightly as λ/d increases.

Chapter 5 CONCLUSIONS AND RECOMMENDATIONS

5.1 Conclusions

A numerical model is set up based on the linear diffraction theory and the eigenfunction expansion method to predict the interaction of a regular small amplitude wave train with a thin permeable vertical barrier. The fluid mechanics within a permeable barrier is studied and the boundary conditions along the barrier's surface are thereby developed. Expressions are obtained for parameters of engineering interest, including the transmission and reflection coefficients, the wave runup on the upwave and downwave sides of the barrier, and the maximum horizontal force and overturning moment on the barrier.

Comparisons have been carried out with previous numerical studies for the limiting cases of an impermeable barrier and a permeable barrier extending down to the seabed, and very close agreement has been obtained in all such cases. A selection of numerical results based on the present method have been presented. These show the transmission, reflection and energy dissipation coefficients, the maximum horizontal force and overturning moment coefficients, as well as the wave runup on the upwave and downwave sides of the barrier as functions of the dimensionless wave frequency kh, the relative penetration of the barrier h/d, and the permeability parameter S. These results exhibit various features of interest, some of which are expected. It is concluded that, the various parameters of interest depend on kh and h/d for a permeable barrier in a similar manner as for a solid barrier, while they also depend significantly on the permeability parameter. Under a specified wave condition, a barrier with a given permeability will give rise to a maximum energy dissipation coefficient. It is also seen that a certain wave condition may produce a maximum horizontal force and overturning moment on the barrier.

As an extension to the present method, another numerical model is set up to predict the wave interactions with a pair of thin permeable vertical barriers fixed above the seabed. The two barriers are identical in permeability and penetration. A selection of numerical

results are presented. The results show the transmission, reflection and energy dissipation coefficients, the maximum horizontal force acting on both the upwave and downwave barriers as functions of the complex barrier permeability parameter S, the wave frequency kh and the dimensionless distance between the barriers λ/d. Under the same wave conditions, the transmission and reflection coefficients in the two-barrier case are smaller than those in the one-barrier case, and the wave energy dissipation coefficient is greater. Thus compared to one-barrier problem, two barriers generate relatively smaller reflection and transmission and dissipate more wave energy. Some resonance occurs under certain wave conditions, which K_t, K_r, K_d and C_F are extraordinarily high or low. Under a certain wave condition, all the values of K_t, K_r, K_d and C_F vary periodically as the distance between the barriers is increased by a quarter of the wave length, and the amplitudes decrease as the permeability of the barriers increases.

The features of the parameters of engineering interest discovered for one or two thin permeable vertical barriers are considered to be meaningful and are hoped to be used to predict wave effects on barrier(s) in practical applications.

5.2 Recommendations for further study

Only the numerical model for the one-barrier problem has been validated against previous numerical results for some limiting conditions. At present no results for the two-barrier problem are available for comparision. To further examine the effectiveness of the numerical models, a wide range of experiments need to be carried out.

The present approach assumes that the barrier is thin and that the fluid velocities along both the barrier surfaces are the same. However, the thickness of the barrier affecting the fluid mechanics within the barrier needs to be investigated more properly.

Finally, further studies in this area are needed to develop numerical models of a single wave barrier under random wave conditions, oblique waves and combined wave-current

conditions. For two or more barriers, different drafts and barrier widths, as well as permeability parameters could be taken into account.

References

Abul-Azm, R.G. (1992). "Water diffraction through submerged breakwaters." *Journal of Waterway, Port, Coastal and Ocean Engineering, ASCE*, **93**(6), 587-605.

Chwang, A.T. (1983). "A porous-wavemaker theory." *Journal of Fluid Mechanics*, **132**, 395-406.

Dalrymple, R.A., Losada, M.A., and Martin, P.A. (1991). "Reflection and transmission from porous structures under oblique wave attack." *Journal of Fluid Mechanics*, **224**, 625-644.

Dalrymple, Robert A and Martin, P.A. (1990). "Wave diffraction through offshore breakwaters." *Journal of Waterway, Port, Coastal and Ocean Engineering, ASCE*, **116**, 727-741.

Gilman, J.F., and Nottingham, D. (1992). "Wave barriers: an environmentally benign alternative." *Proceeding of the Conference of Coastal Engineering Practice '92 , ASCE,* 479-486

Isaacson, M. (1996). "Simplified estimation of wave effects on vertical barriers." *Journal of Waterway, Port, Coastal and Ocean Engineering, ASCE*, submitted.

Kondo, H. (1979). "Analysis of breakwaters having two porous walls." *Coastal Structures, ASCE*, 79 , 962-977.

Le Méhauté, B. (1972). "Progressive wave absorber." *Journal of Hydraulic Research, IAHR*, **10**(2), 153-169.

Liu, P. L-F., and Abbaspour, M. (1982). "Wave scattering by a rigid thin barrier." *Journal of Waterway, Port, Coastal and Ocean Engineering, ASCE*, **108**(4), 479-491.

Losada, I.J., Losada, M.A., and Baquerizo, A. (1993). "An analytical method to evaluate the efficiency of porous screen as wave dampers." *Applied Ocean Research*, **15**, 207-215.

Losada, I.J., Losada, M.A., and Roldan, A.J. (1992). "Propagation of oblique incident waves past rigid vertical thin barriers." *Applied Ocean Research*, **14**, 191-199.

Macaskill, C. (1979). "Reflection of water waves by a permeable barrier." *Journal of Fluid Mechanics*, **95**, 141-157.

Madsen, O.S. (1974). "Wave transmission through porous structures." *Journal of Waterway, Port, Coastal and Ocean Engineering, ASCE*, **100**, 169-188.

Madsen, P.A. (1983). "Wave reflection from a vertical permeable wave absorber." *Coastal Engineering*, **7**, 381-396.

Mallayachari, V., and Sundar, V. (1994). "Reflection characteristics of permeable seawalls." *Coastal Engineering*, **23**, 135-150.

Mei, C.C.(1985). "Resonant reflection of surface water waves by periodic sand bars." *Journal of Fluid Mechanics*, **152**, 315-335.

Naciri, M., and Mei, C.C. (1988). "Bragg scattering of water waves by a doubly periodic seabed." *Journal of Fluid Mechanics*, **192**, 51-74.

Sollitt. C.K., and Cross, R.H. (1972). "Wave transmission through permeable breakwaters." *Proceedings of the 13th Coastal Engineering Conference, ASCE,* Vancouver, B.C, Canada, 1827-1846.

Twu, S.W., and Lin, D.T. (1990). "On highly effective wave absorber." *Coastal Engineering*, **15**, 389-405.

Twu, S.W., and Lin, D.T. (1990). "Wave reflection by a number of thin porous plates fixed in a semi-infinitely long flume." *Proceedings of the 22nd Coastal Engineering Conference, ASCE,* Delft, The Netherlands, 1046-1059.

Yu, Xiping (1995). "Diffraction of water waves by porous breakwaters." *Journal of Waterway, Port, Coastal and Ocean Engineering, ASCE,* **121**, 275-282.

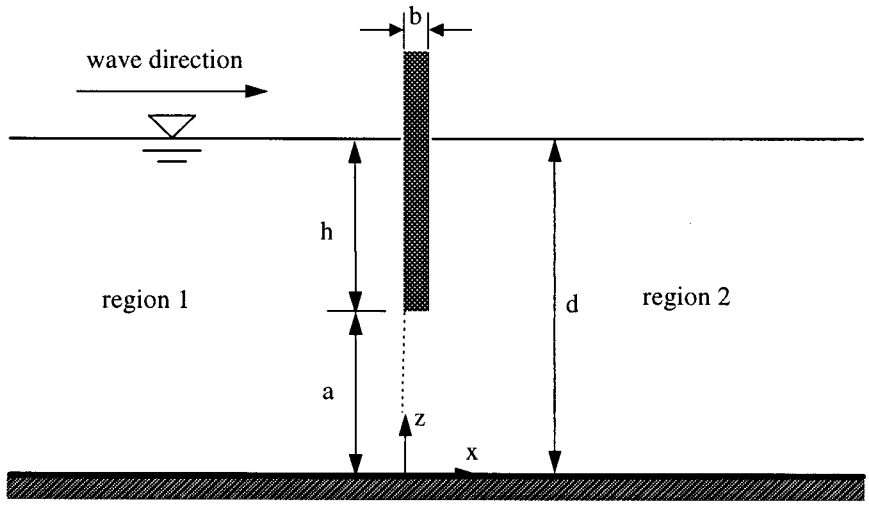

Figure 1 Definition sketch of one-barrier problem.

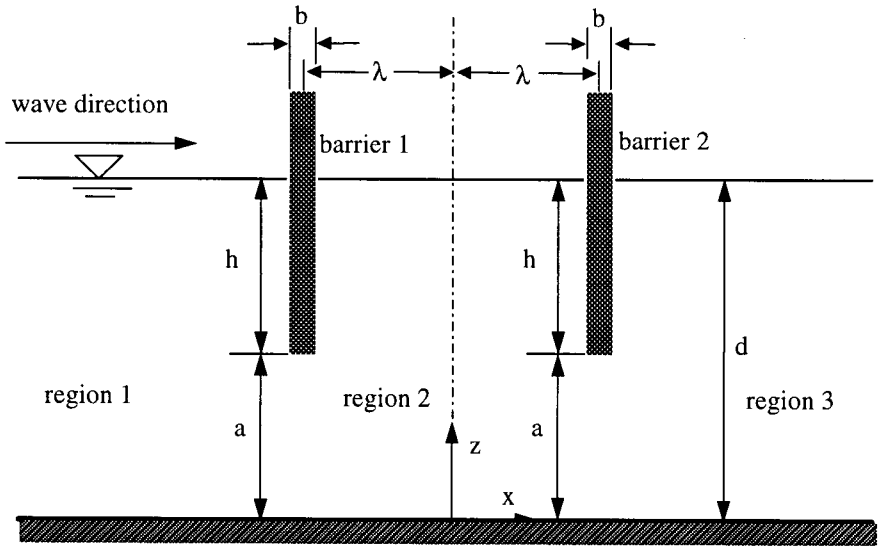

Figure 2 Definition sketch of two-barrier problem.

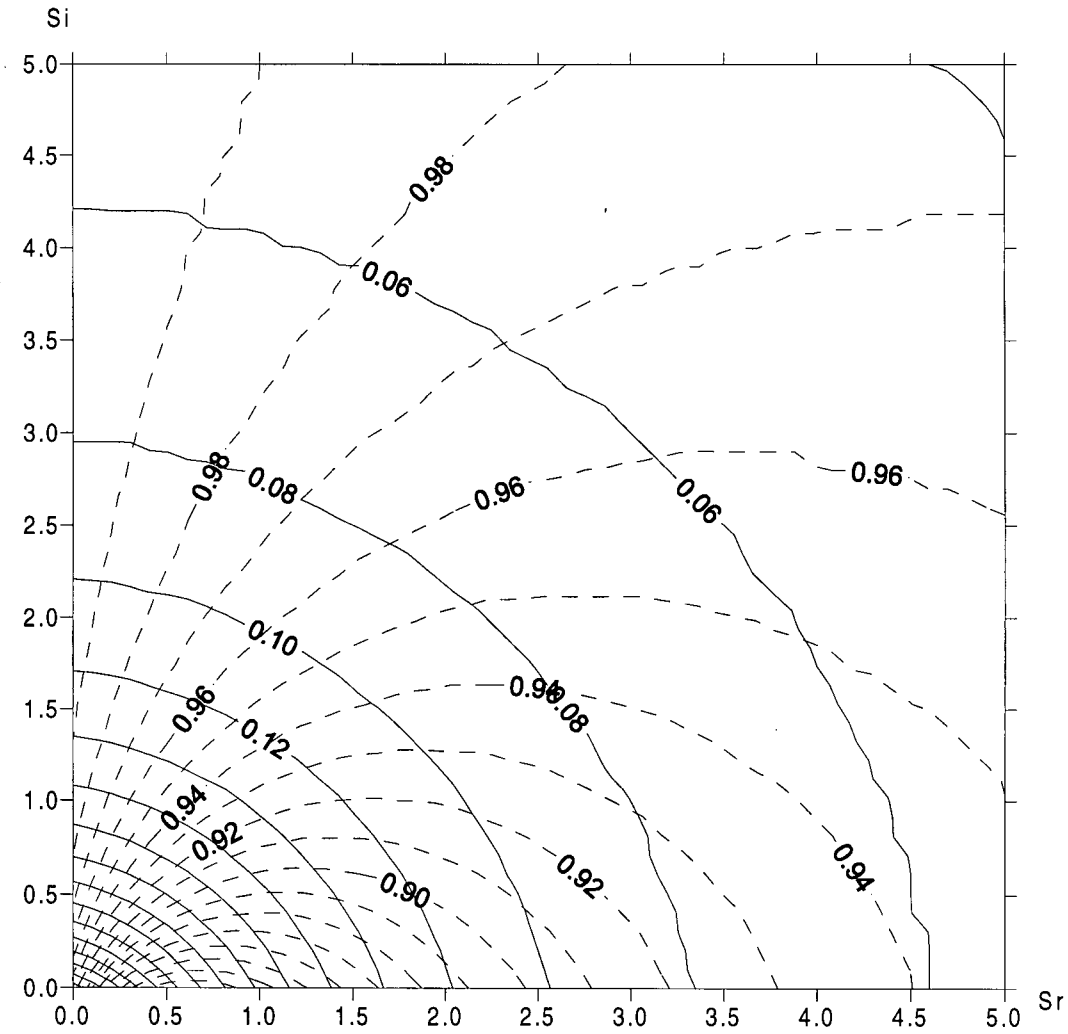

Figure 3 Transmission and reflection coefficients shown as contours in the complex S plane for the case $h/d = 0.5$, $kh = 0.5$ (one-barrier problem). ———, K_r; -------, K_t.

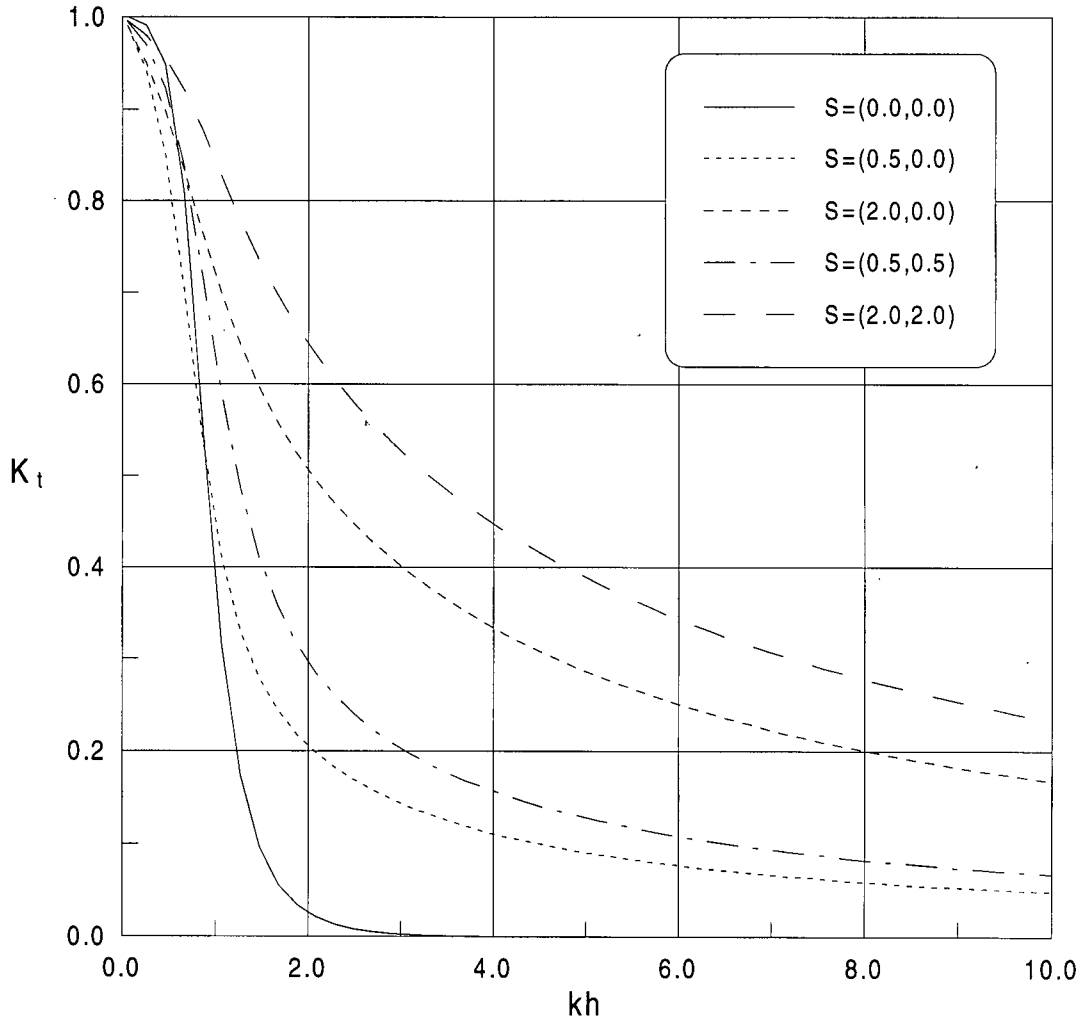

Figure 4 Transmission coefficient as a function of kh for $h/d = 0.5$ and for various values of S (one-barrier problem).

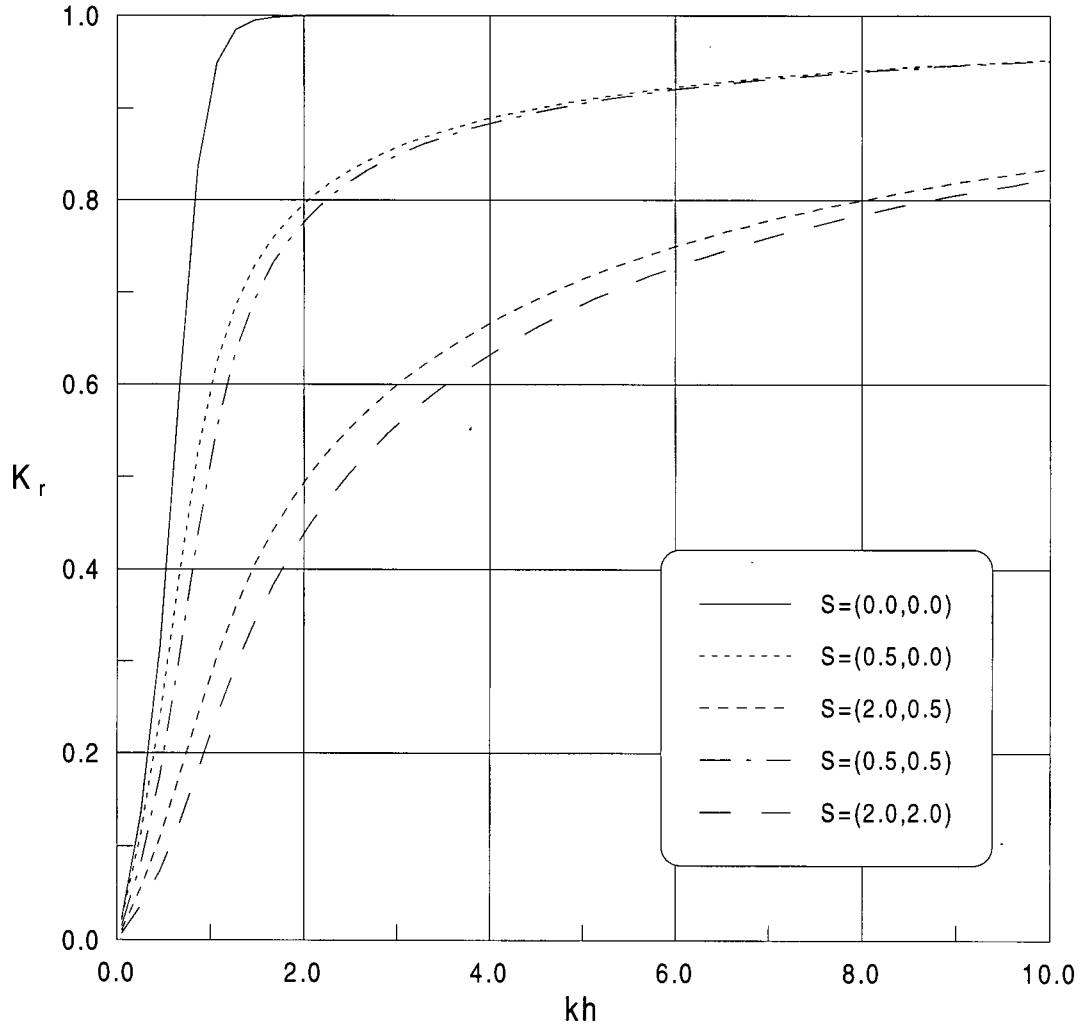

Figure 5 Reflection coefficient as a function of kh for $h/d = 0.5$ and for various values of S (one-barrier problem).

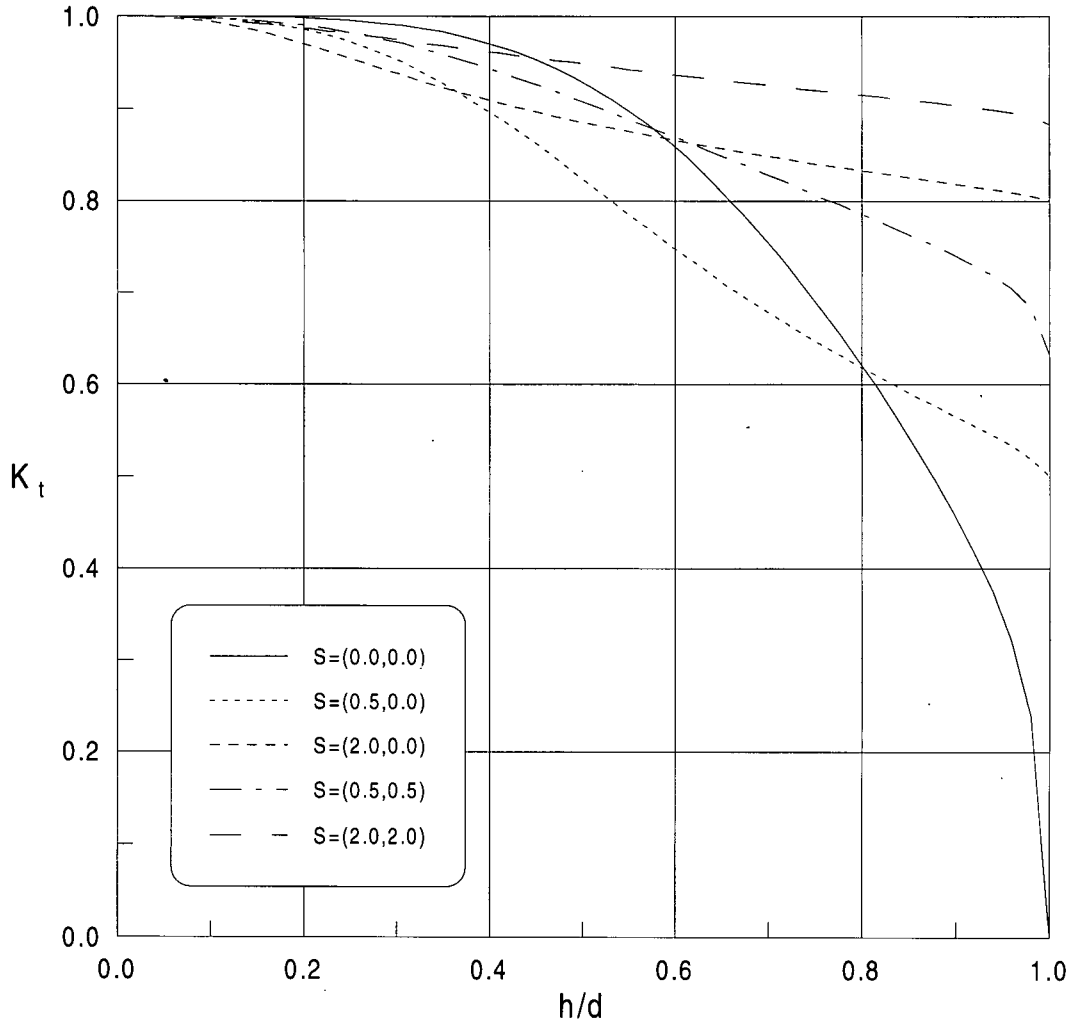

Figure 6 Transmission coefficient as a function of h/d for kd = 1.0 and for various values of S (one-barrier problem).

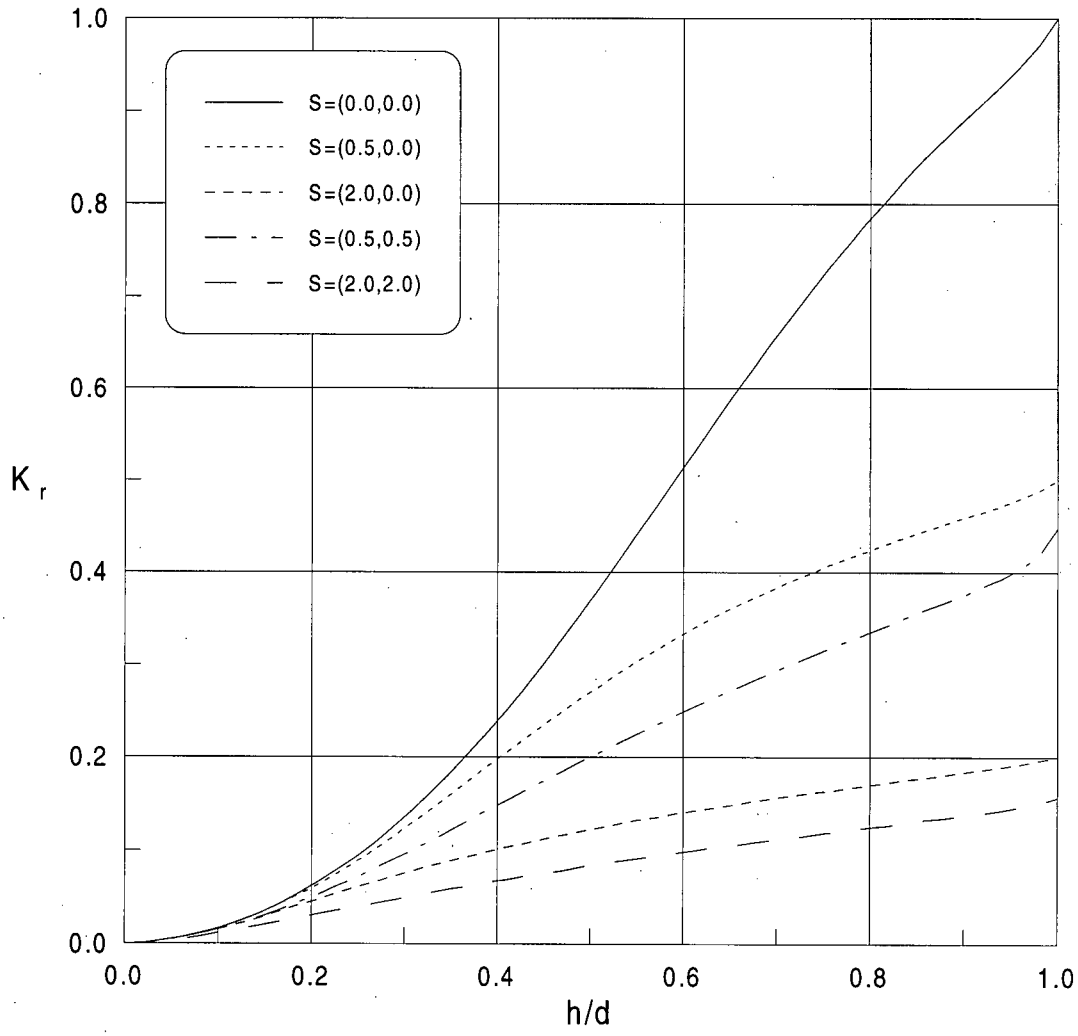

Figure 7 Reflection coefficient as a function of h/d for kd = 1.0 and for various values of S (one-barrier problem).

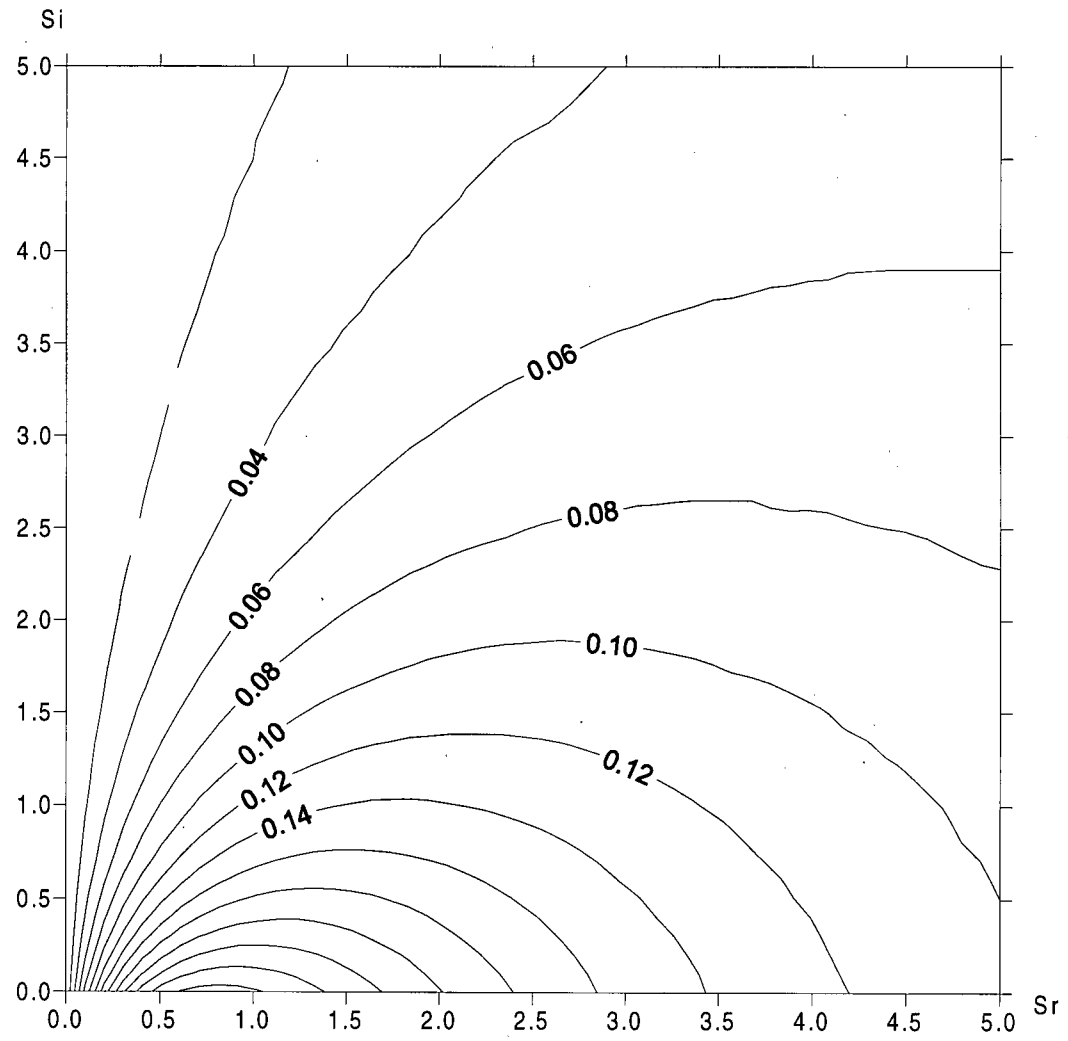

Figure 8 Energy dissipation coefficient shown as contours in the complex S plane for the case $h/d = 0.5$, $kh = 0.5$ (one-barrier problem).

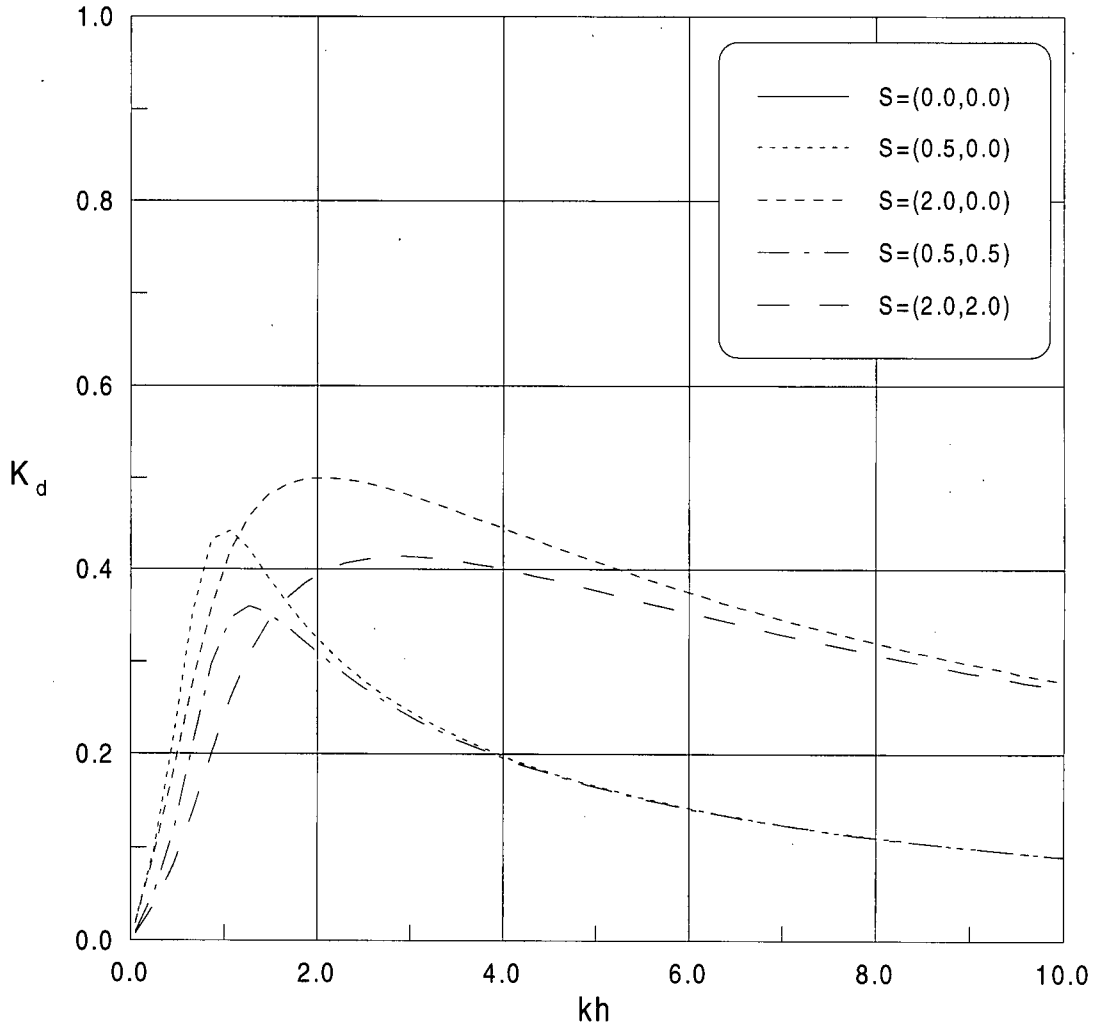

Figure 9 Energy dissipation coefficient as a function of kh for $h/d = 0.5$ and for various values of S (one-barrier problem).

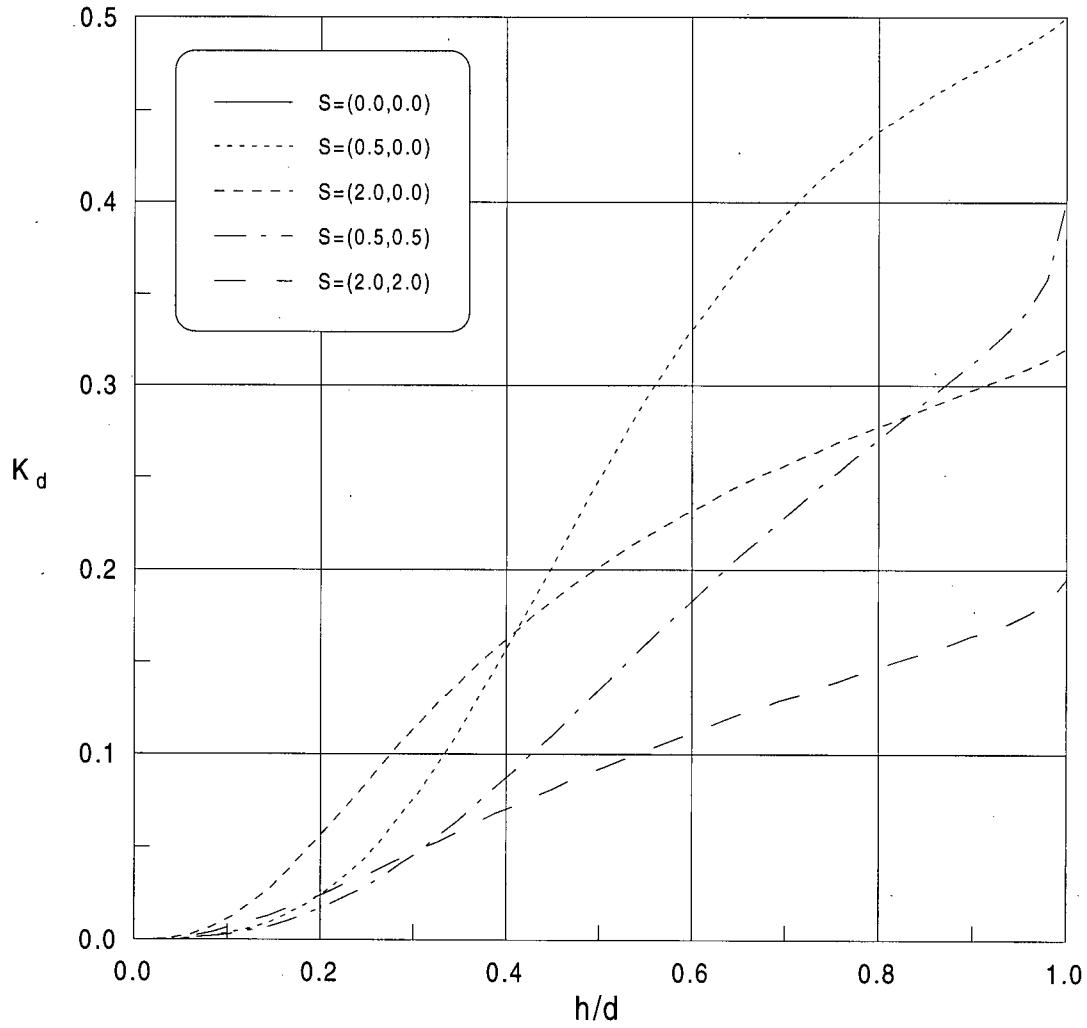

Figure 10 Energy dissipation coefficient as a function of h/d for kd = 1.0 and for various values of S (one-barrier problem).

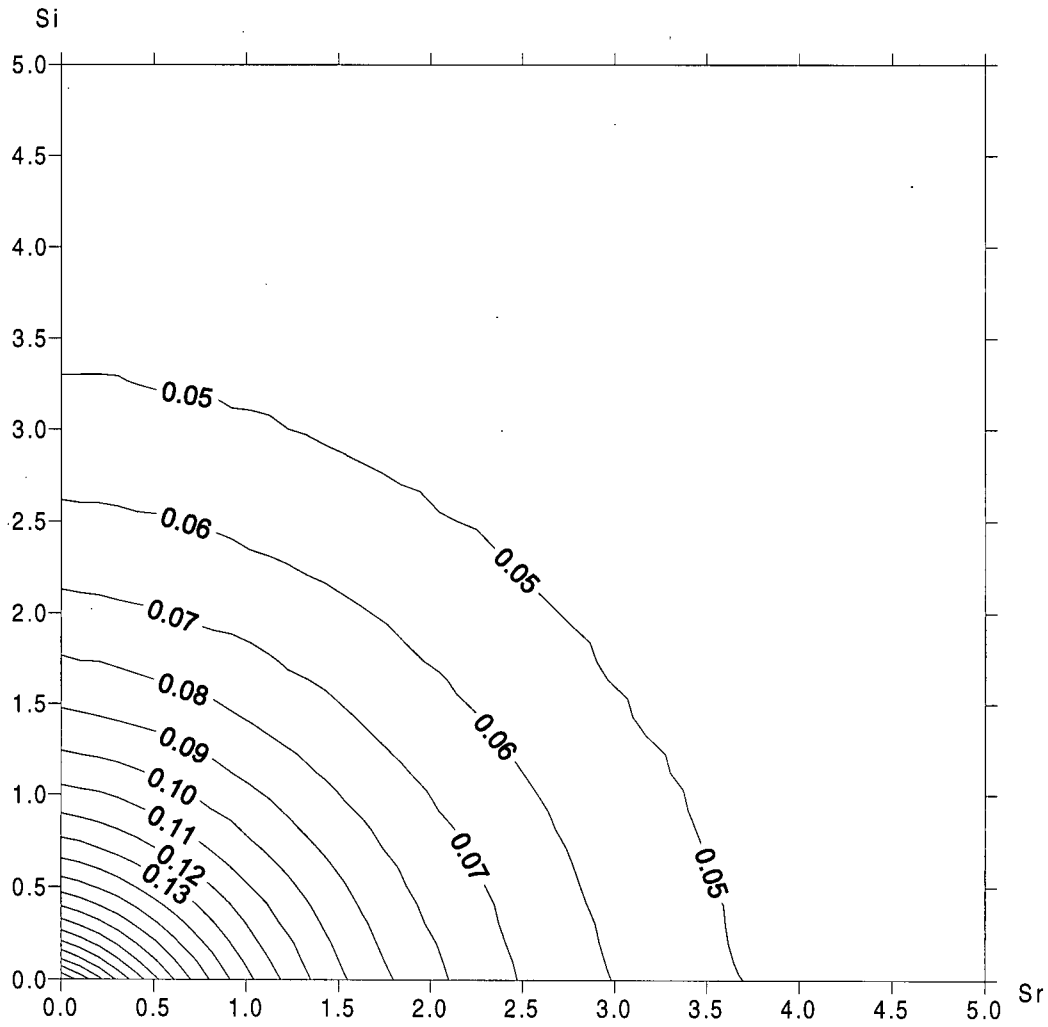

Figure 11 Force coefficient shown as contours in the complex S plane for the case $h/d = 0.5$, $kh = 0.5$ (one-barrier problem).

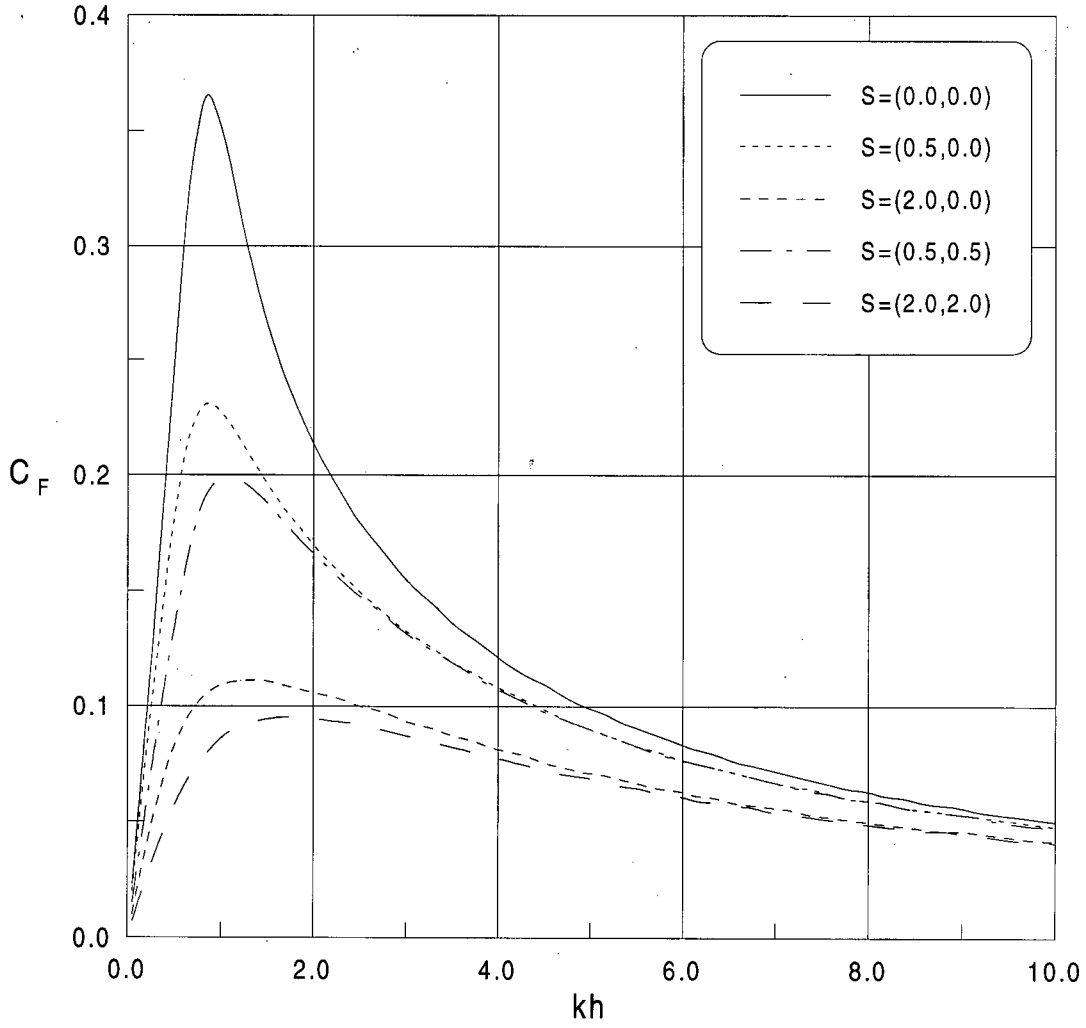

Figure 12 Force coefficient as a function of kh for $h/d = 0.5$ and for various values of S (one-barrier problem).

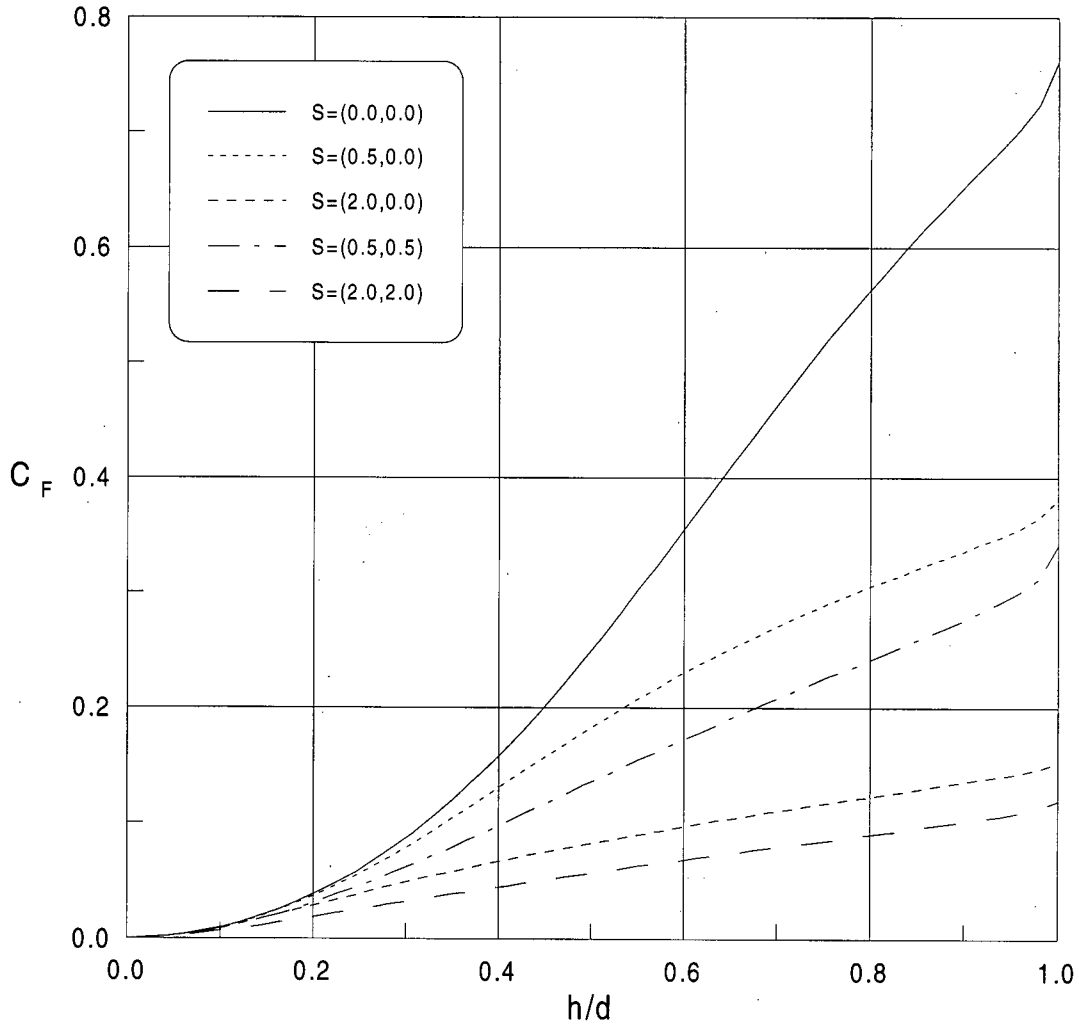

Figure 13 Force coefficient as a function of h/d for kd = 1.0 and for various values of S (one-barrier problem).

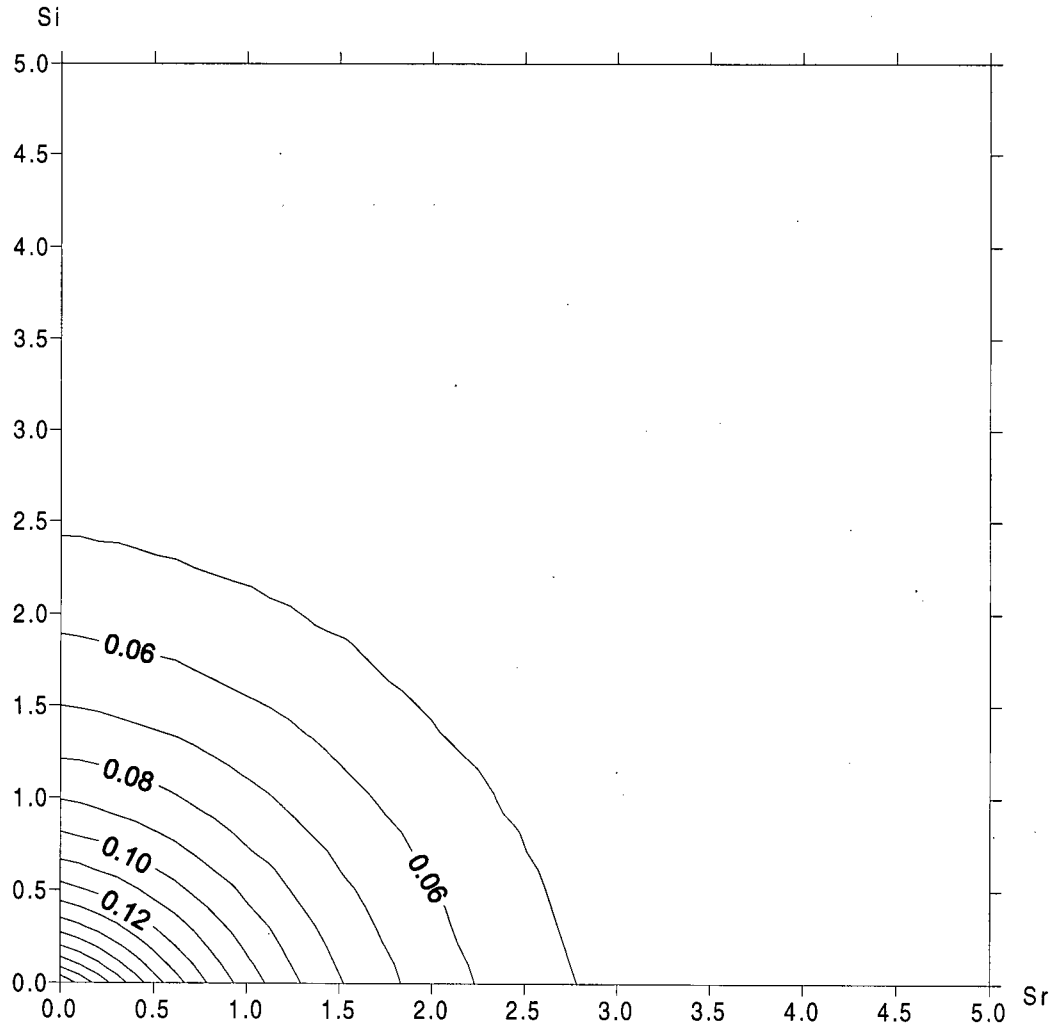

Figure 14 Overturning moment coefficient shown as contours in the complex S plane for the case $h/d = 0.5$, $kh = 0.5$ (one-barrier problem).

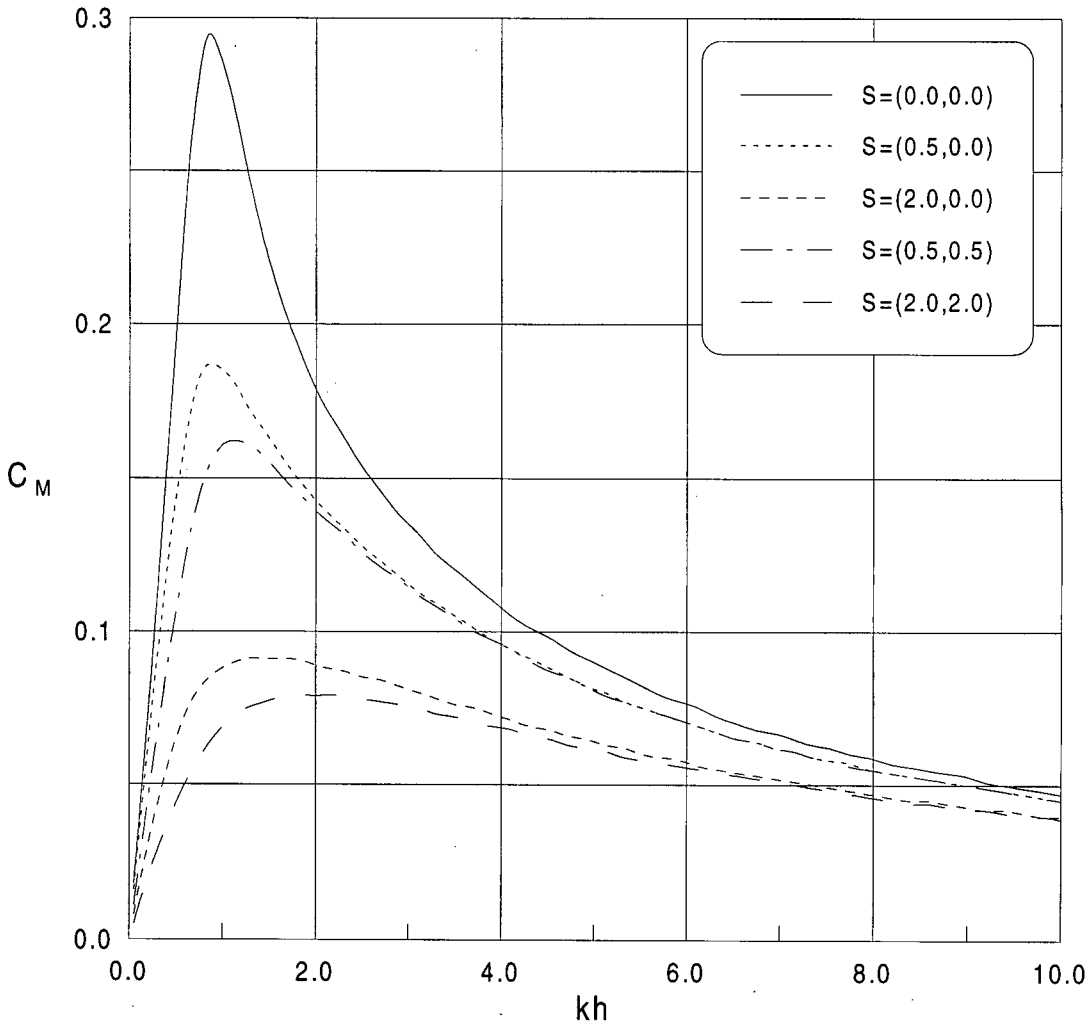

Figure 15 Overturning moment coefficient as a function of kh for $h/d = 0.5$ and for various values of S (one-barrier problem).

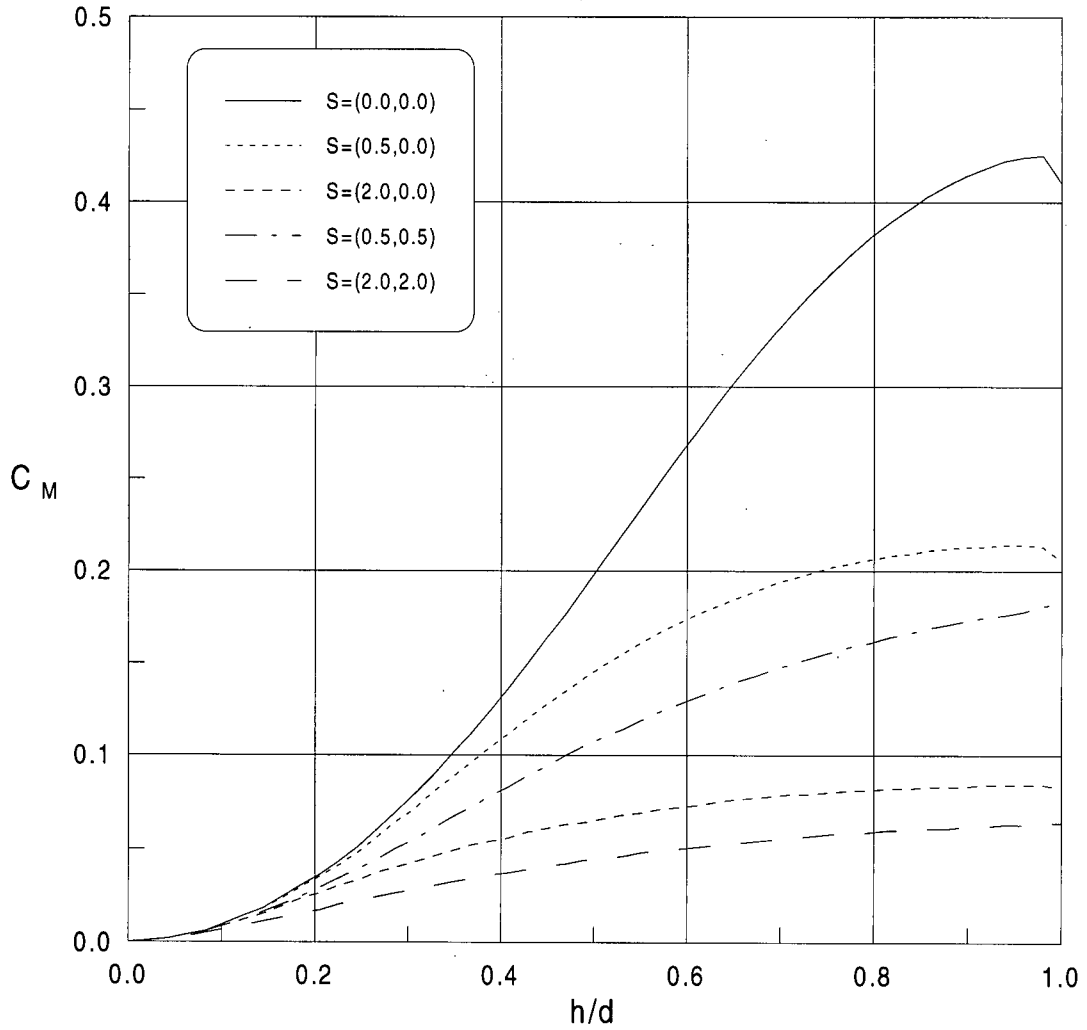

Figure 16 Overturning moment coefficient as a function of h/d for kd = 1.0 and for various values of S (one-barrier problem).

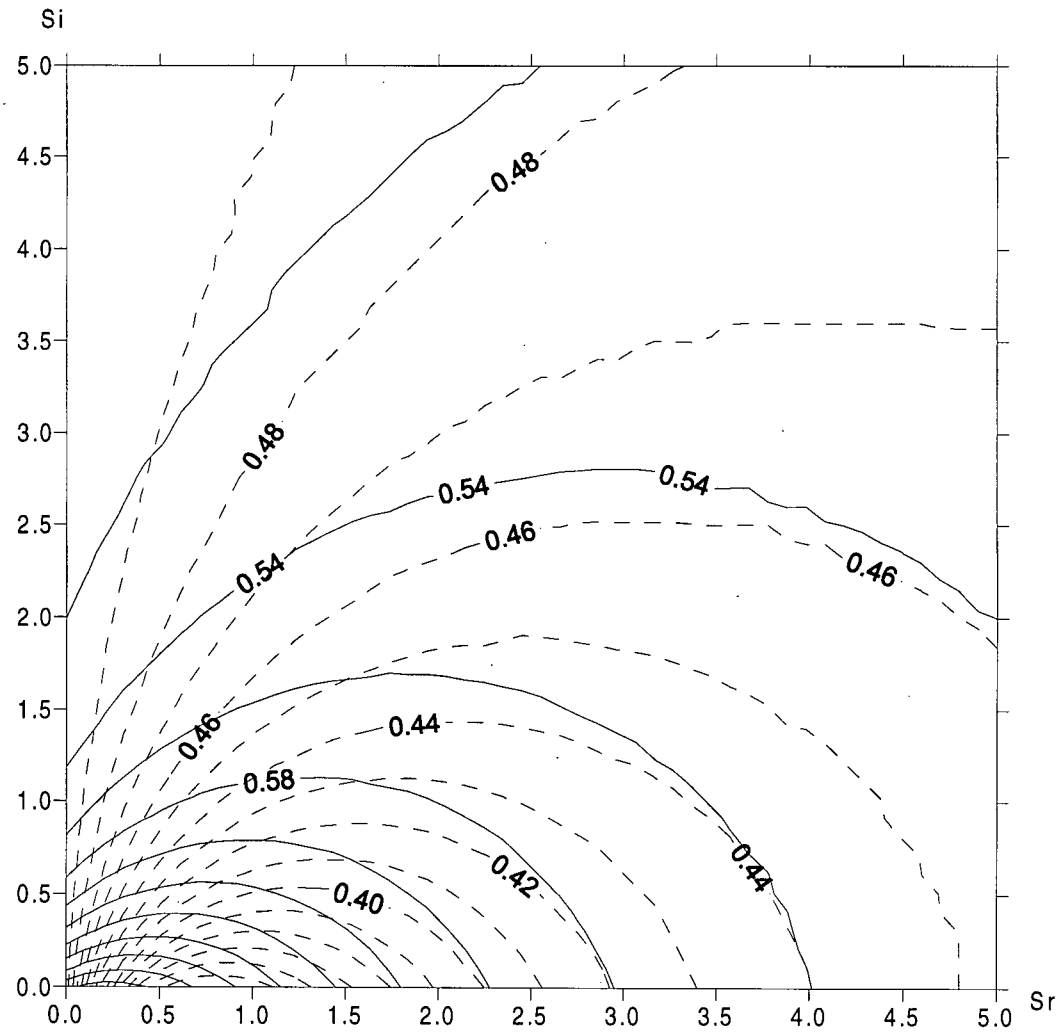

Figure 17 Wave runup coefficients shown as contours in the complex S plane for the case h/d = 0.5, kh = 0.5 (one-barrier problem). ———, R_-/H (upwave); ------ ,R_+/H (downwave).

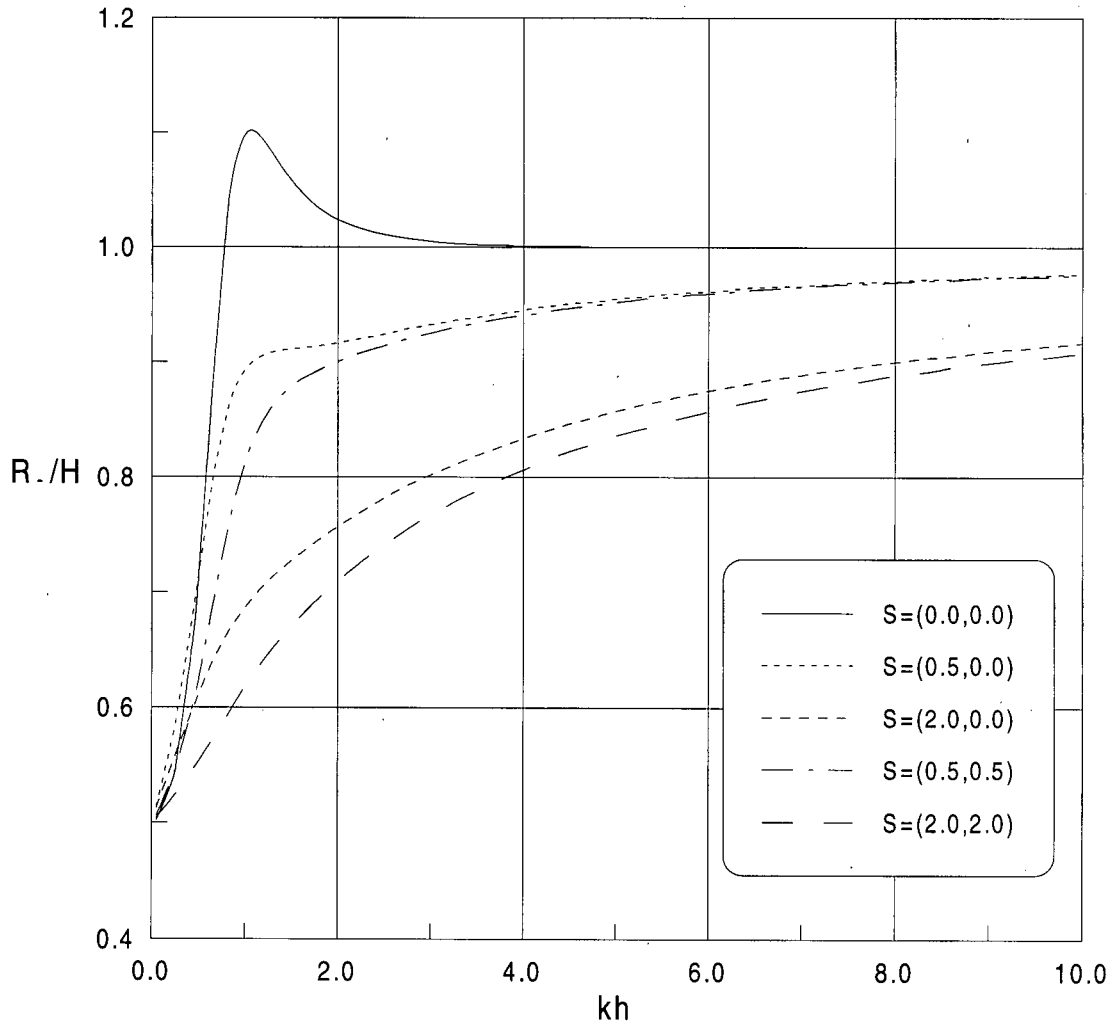

Figure 18 Wave runup (upwave) coefficient as a function of kh for $h/d = 0.5$ and for various values of S (one-barrier problem).

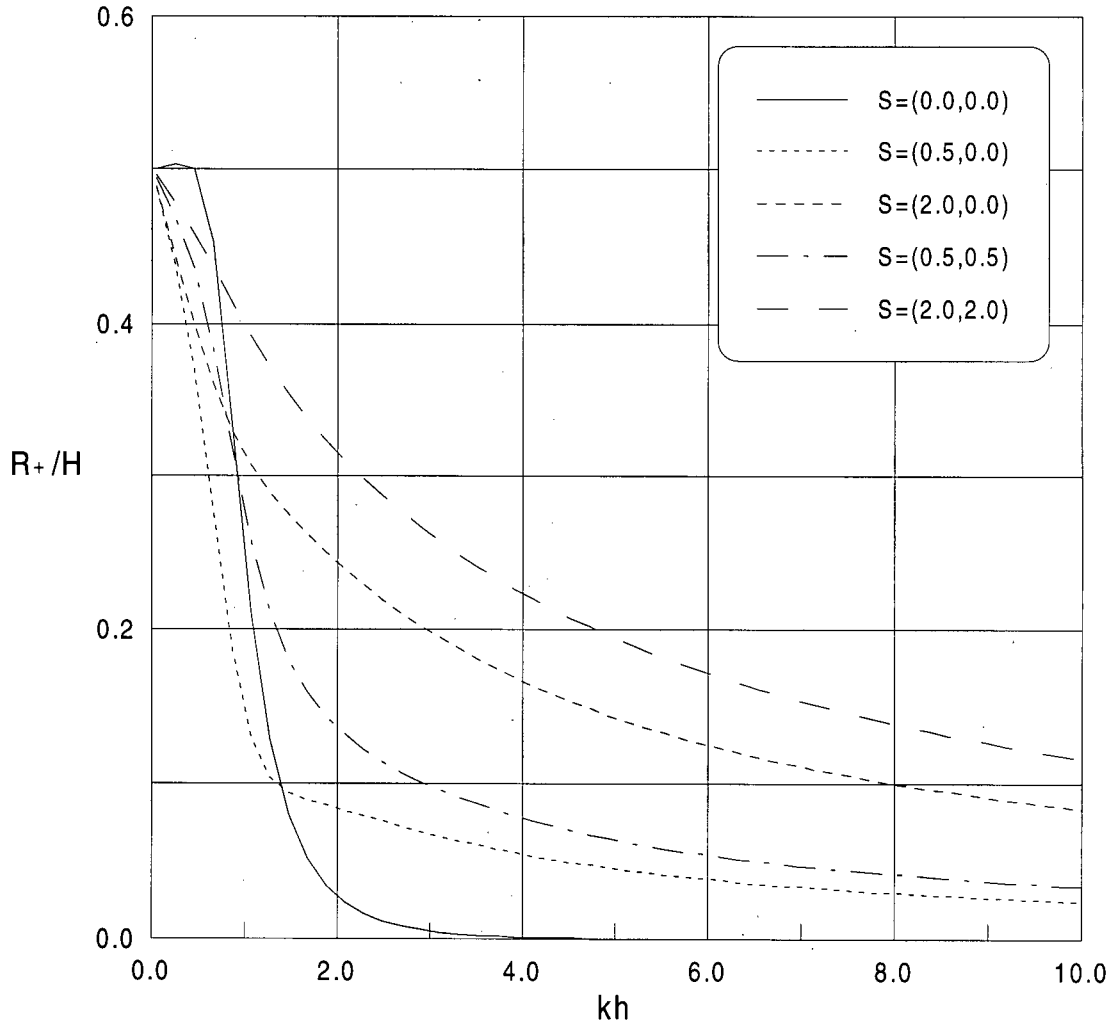

Figure 19 Wave runup (downwave) coefficient as a function of kh for $h/d = 0.5$ and for various values of S (one-barrier problem).

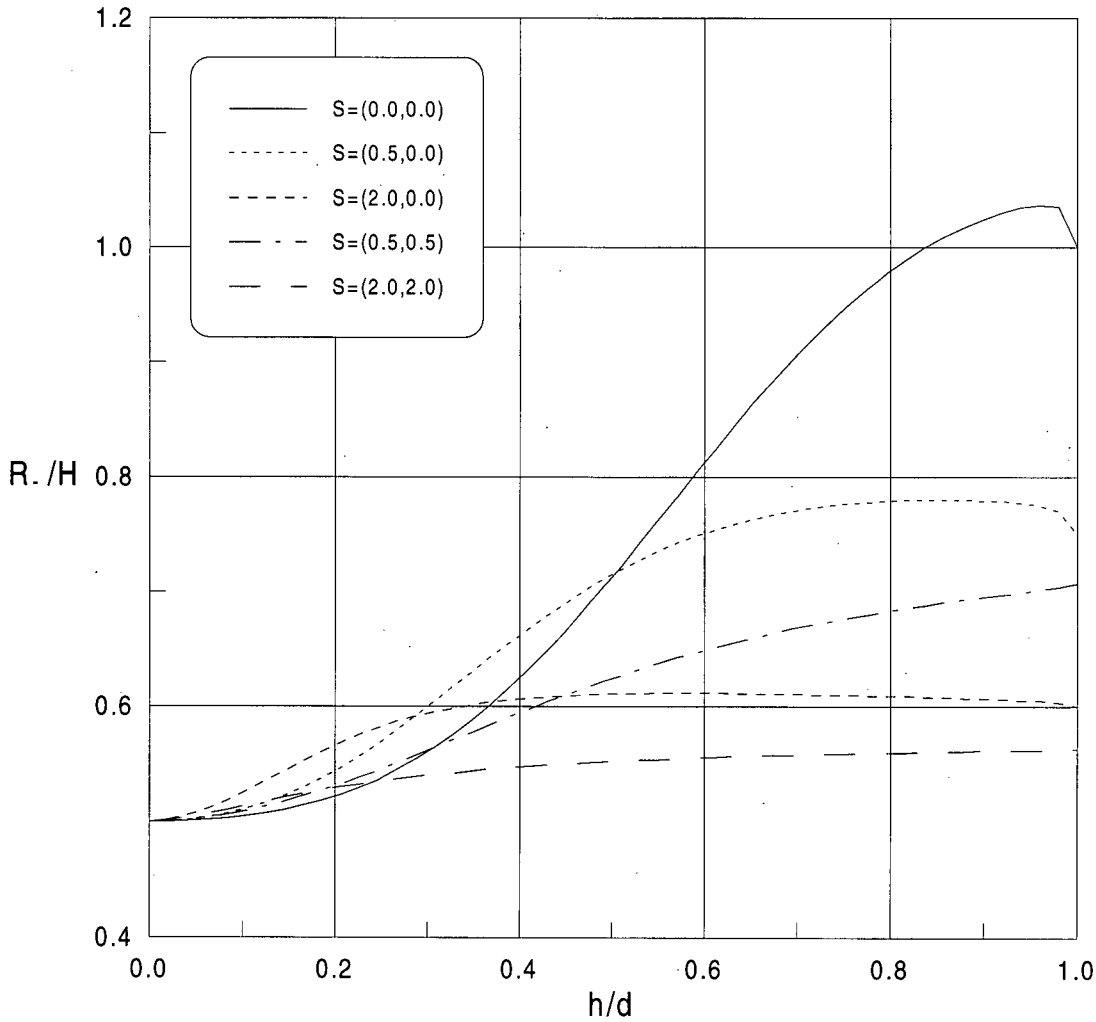

Figure 20 Wave runup (upwave) coefficient as a function of h/d for kd = 1.0 and for various values of S (one-barrier problem).

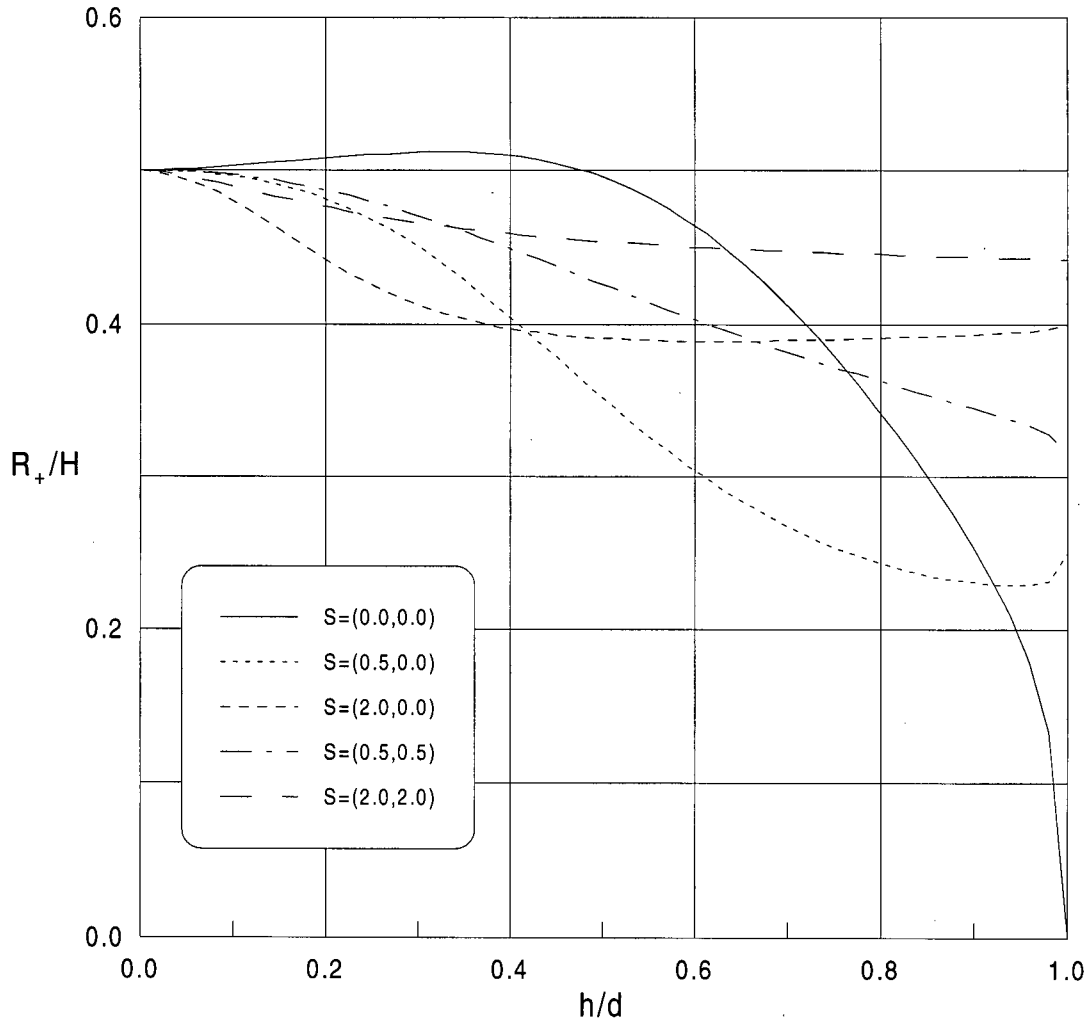

Figure 21 Wave runup (downwave) coefficient as a function of h/d for kd = 1.0 and for various values of S (one-barrier problem).

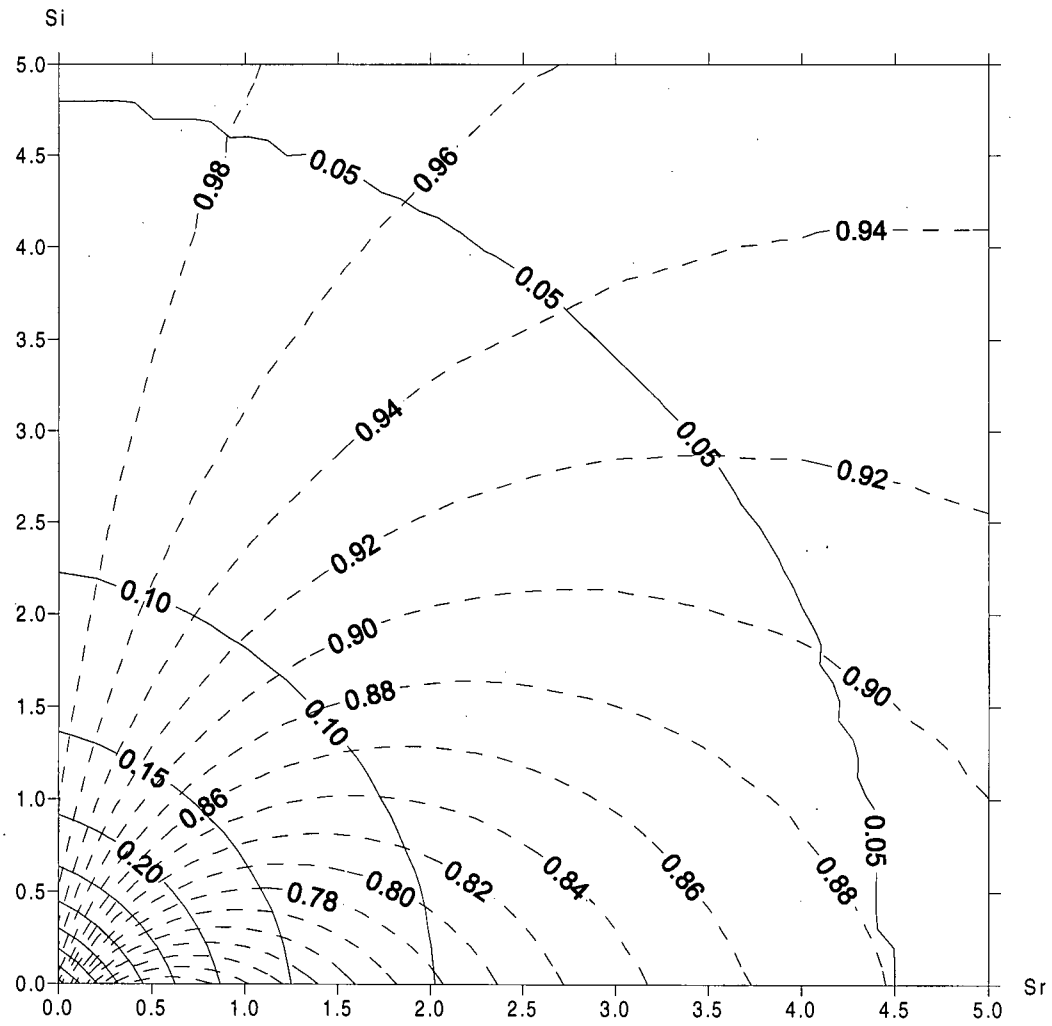

Figure 22 Transmission and reflection coefficients shown as contours in the complex S plane for the case $h/d = 0.5$, $kh = 0.5$, $\lambda/d = 1.0$ (two-barrier problem). ———, K_r; - - - - - - - -, K_t.

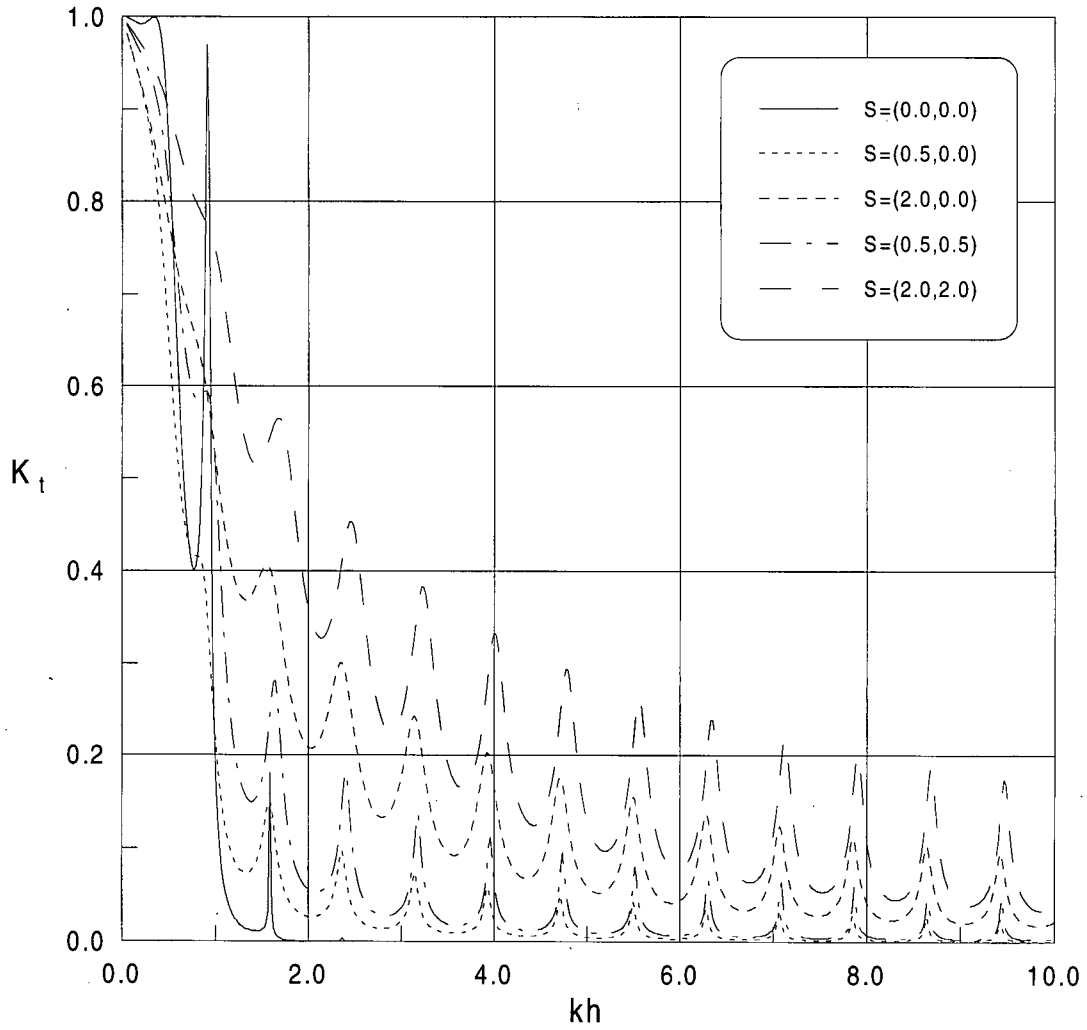

Figure 23 Transmission coefficient as a function of kh for $h/d = 0.5$, $\lambda/d = 1.0$ and for various values of S (two-barrier problem).

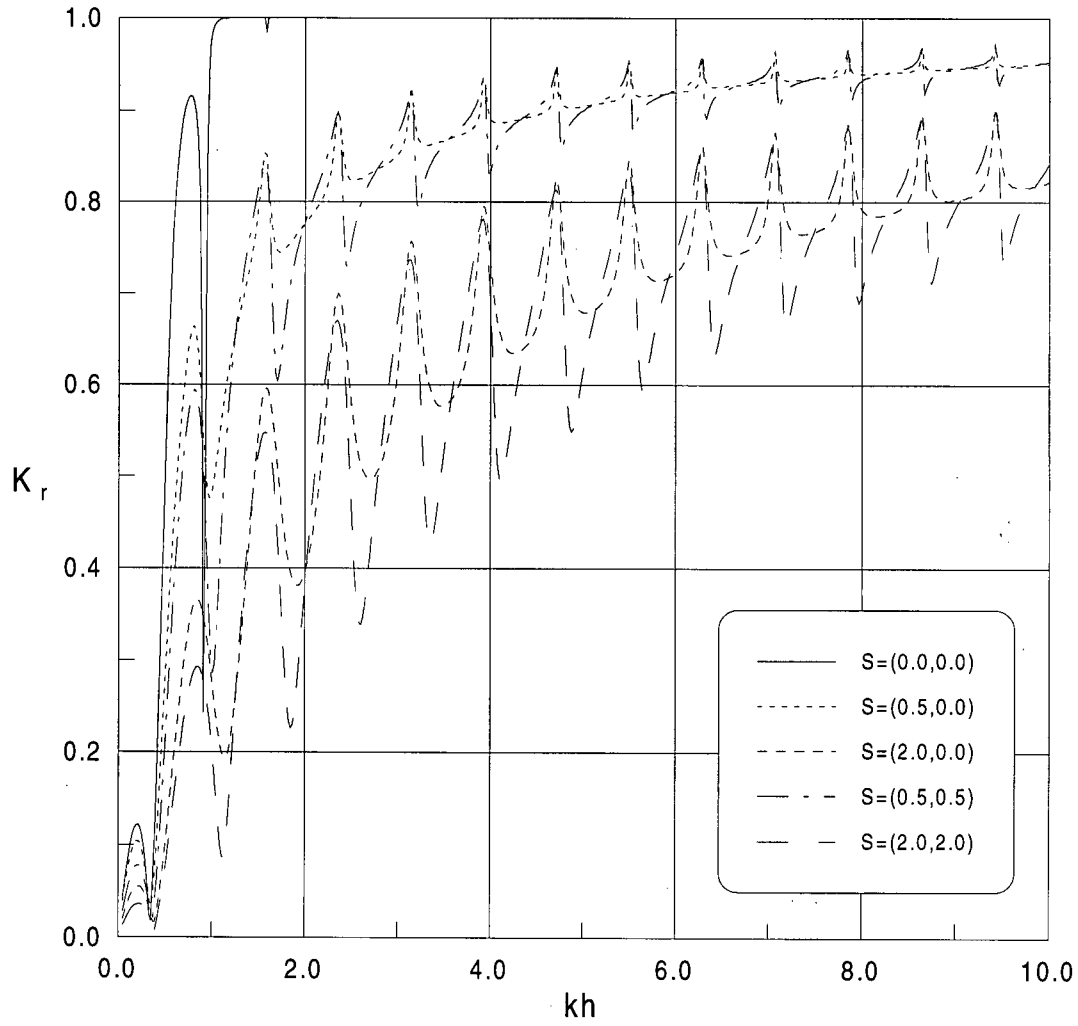

Figure 24 Reflection coefficient as a function of kh for $h/d = 0.5$, $\lambda/d = 1.0$ and for various values of S (two-barrier problem).

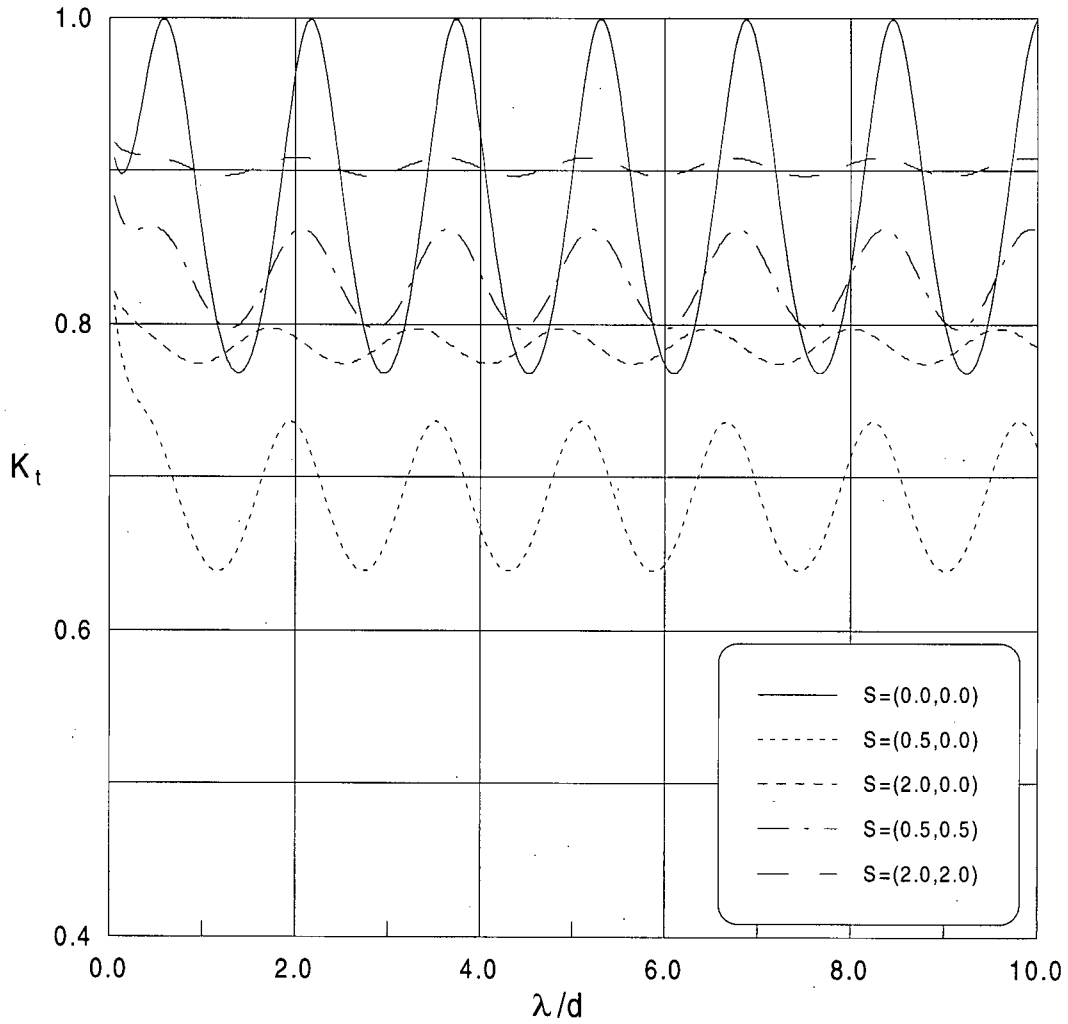

Figure 25 Transmission coefficient as a function of λ/d for $h/d = 0.5$, $kd = 1.0$ and for various values of S (two-barrier problem).

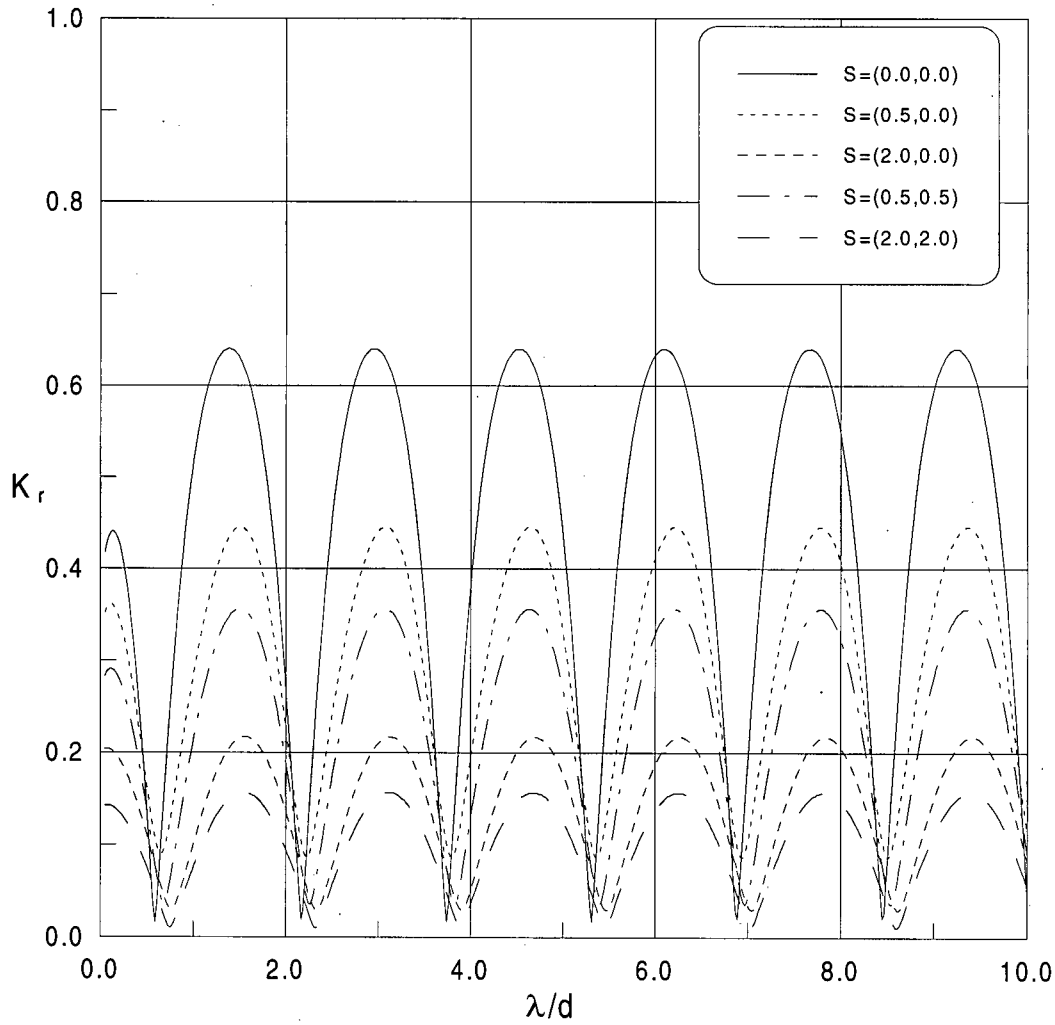

Figure 26 Reflection coefficient as a function of λ/d for $h/d = 0.5$, $kd = 1.0$ and for various values of S (two-barrier problem).

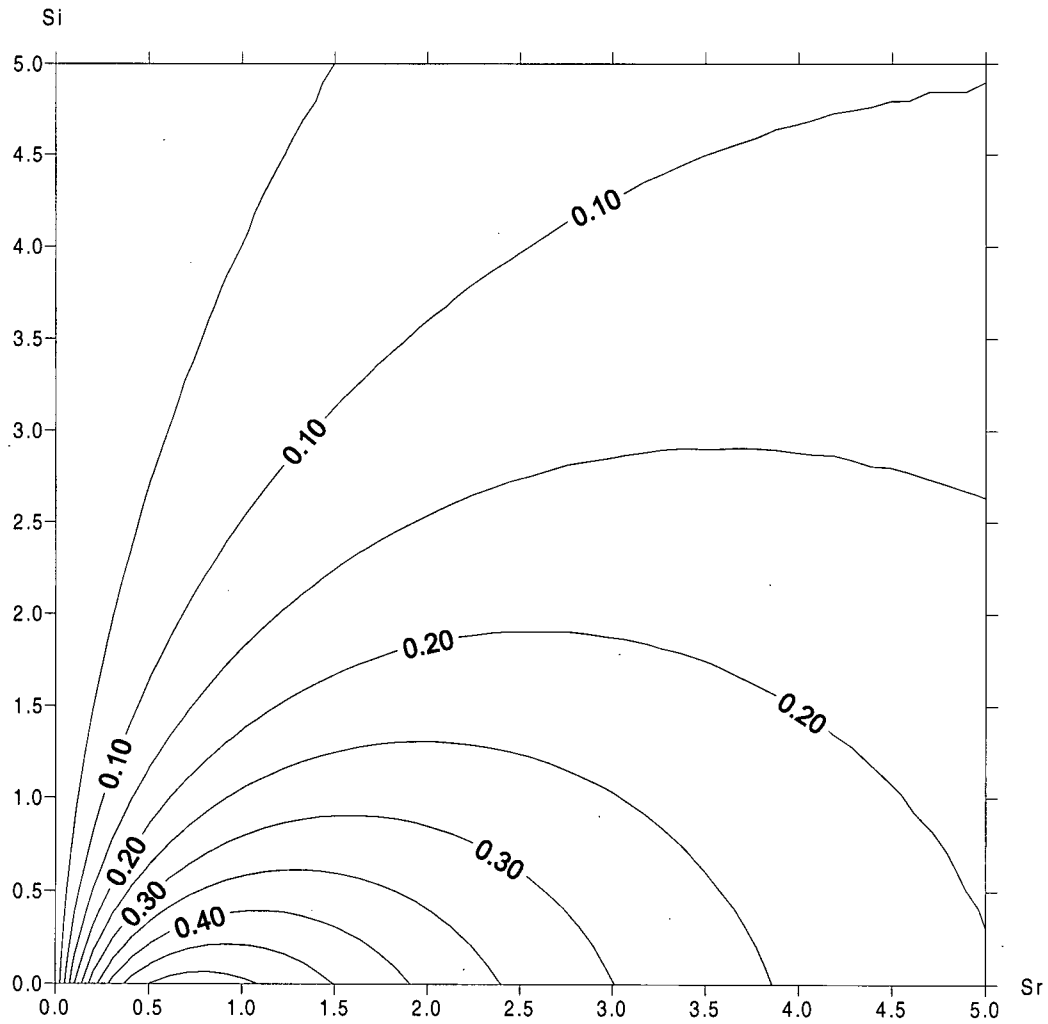

Figure 27 Energy dissipation coefficient shown as contours in the complex S plane for the case $h/d = 0.5$, $kh = 0.5$, $\lambda/d = 1.0$ (two-barrier problem).

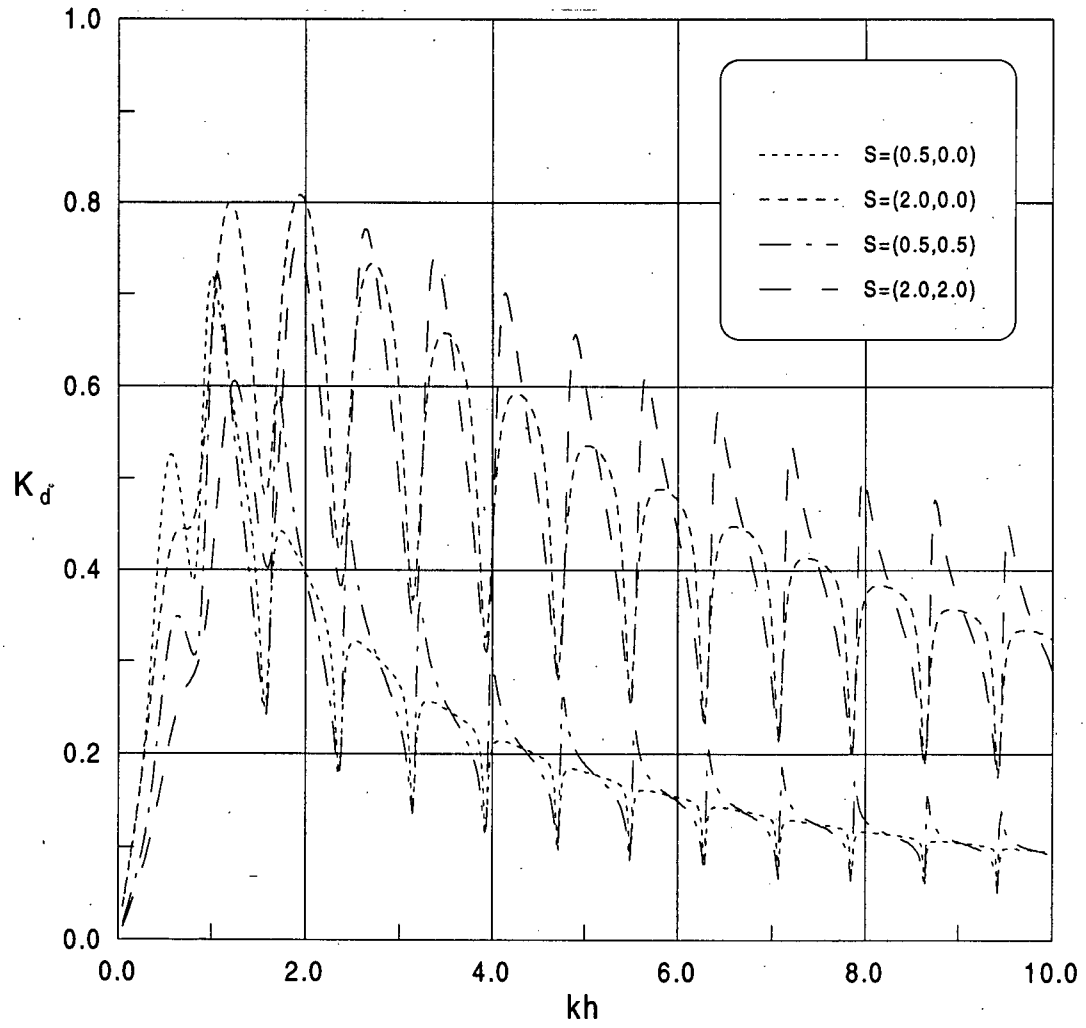

Figure 28 Energy dissipation coefficient as a function of kh for $h/d = 0.5$, $\lambda/d = 1.0$ and for various values of S (two-barrier problem).

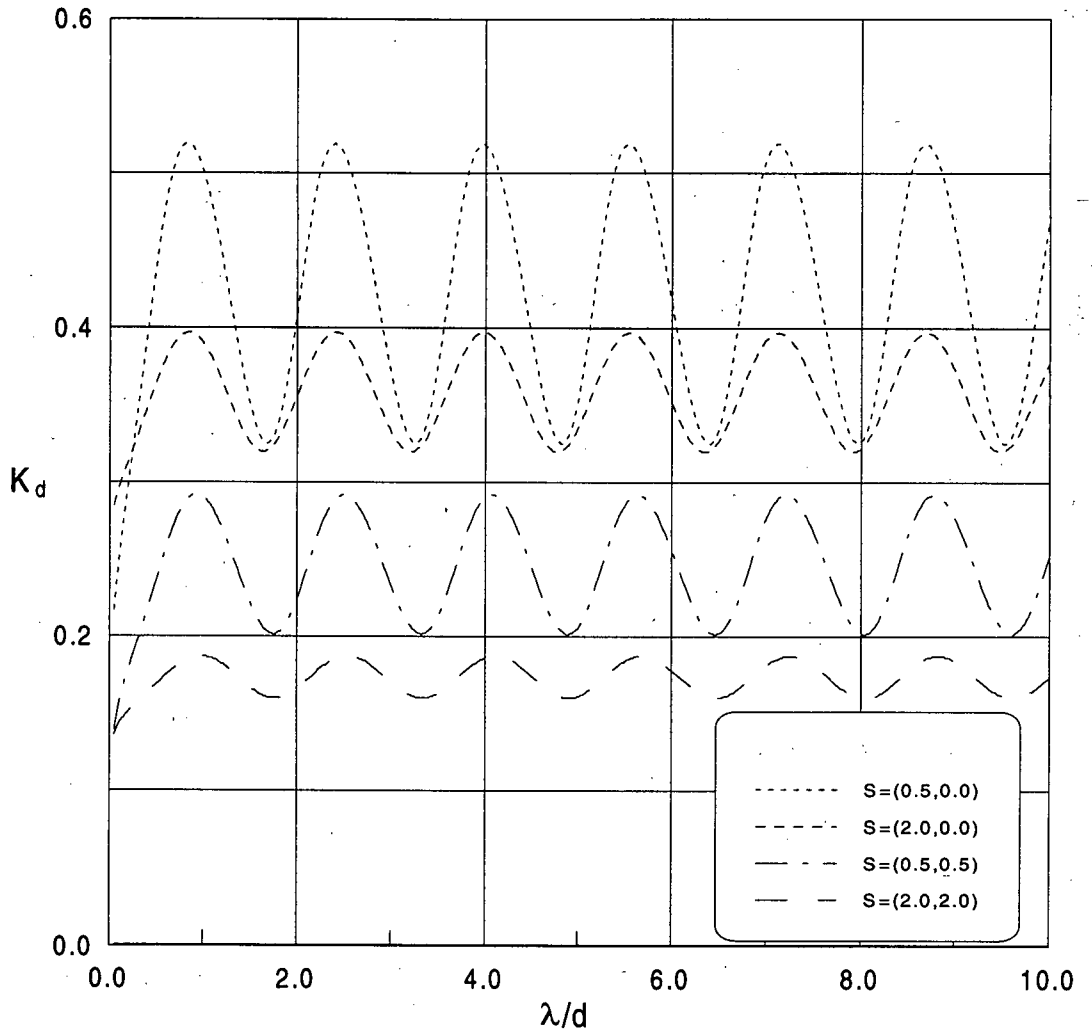

Figure 29 Energy dissipation coefficient as a function of λ/d for $h/d = 0.5$, $kd = 1.0$ and for various values of S (two-barrier problem).

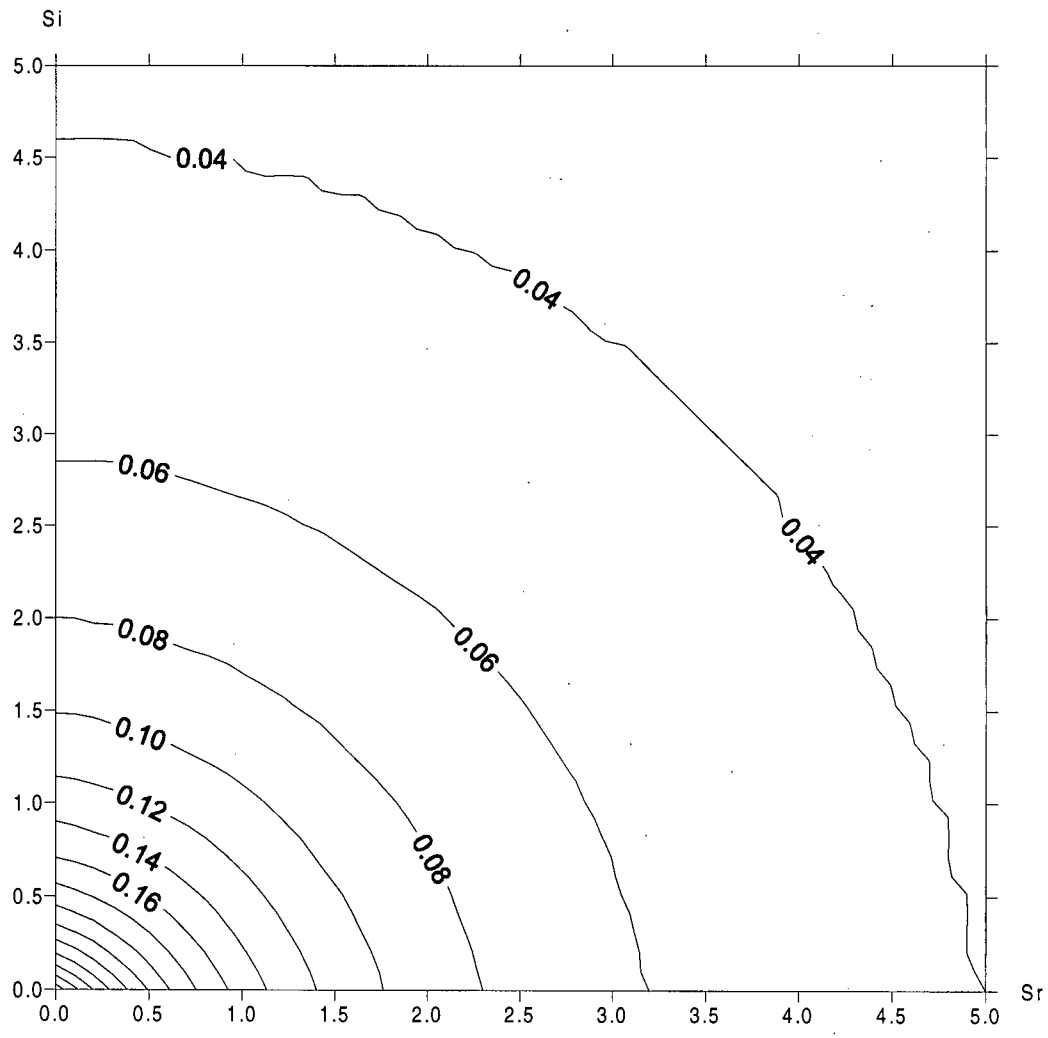

Figure 30 Force coefficients of the upwave barrier shown as contours in the complex S plane for the $h/d = 0.5$, $kh = 0.5$, $\lambda/d = 1.0$ (two-barrier problem).

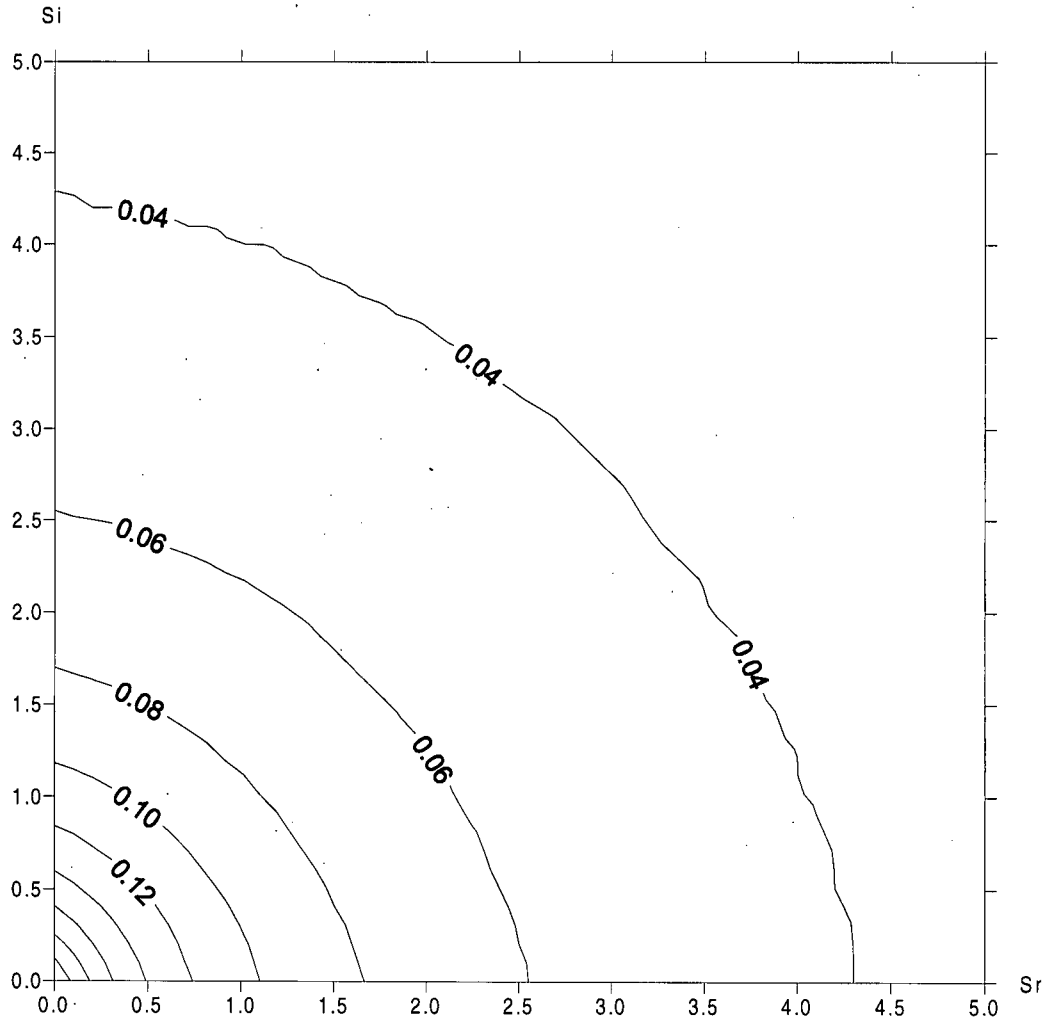

Figure 31 Force coefficients of the downwave barrier shown as contours in the complex S plane for the case $h/d = 0.5$, $kh = 0.5$, $\lambda/d = 1.0$ (two-barrier problem).

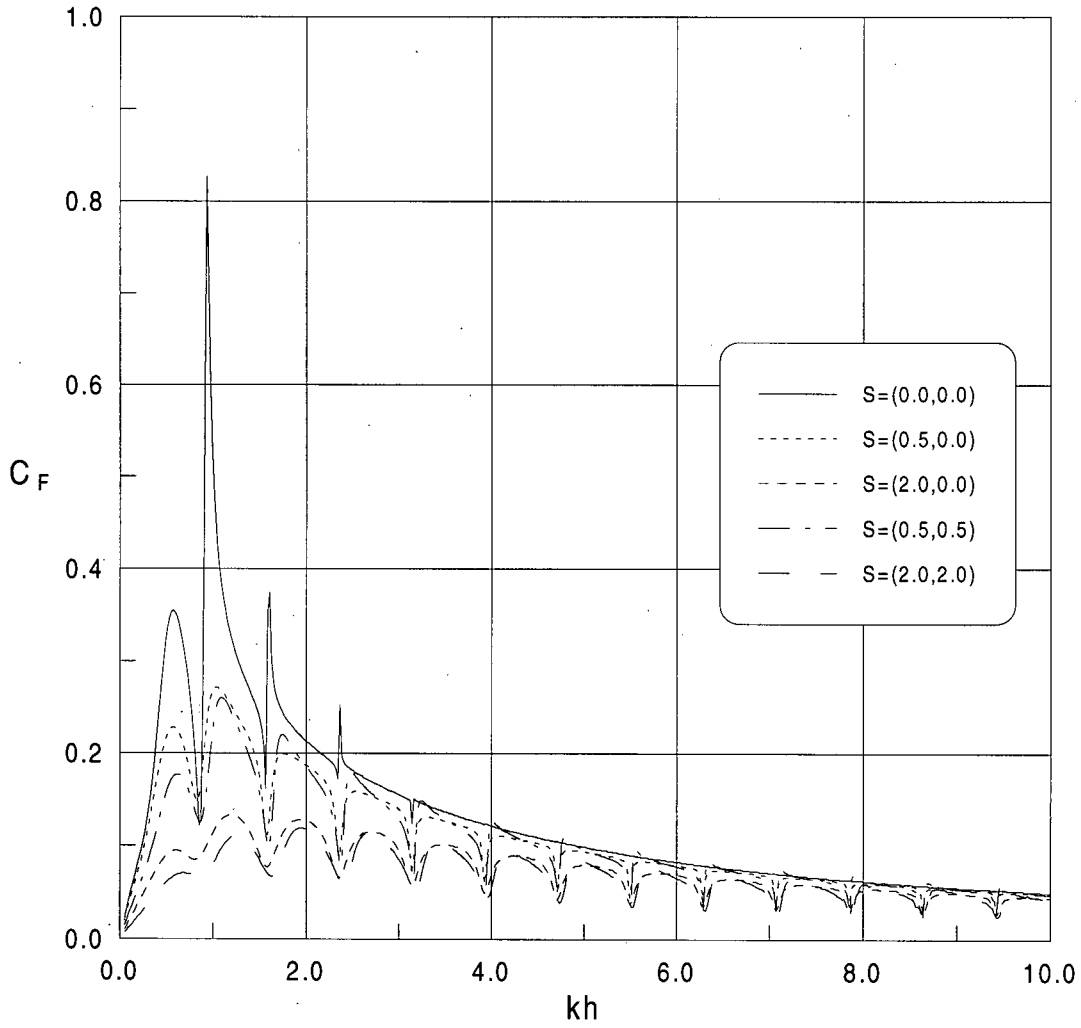

Figure 32 Force coefficient of the upwave barrier as a function of kh for $h/d = 0.5$, $\lambda/d = 1.0$ and for various values of S (two-barrier problem).

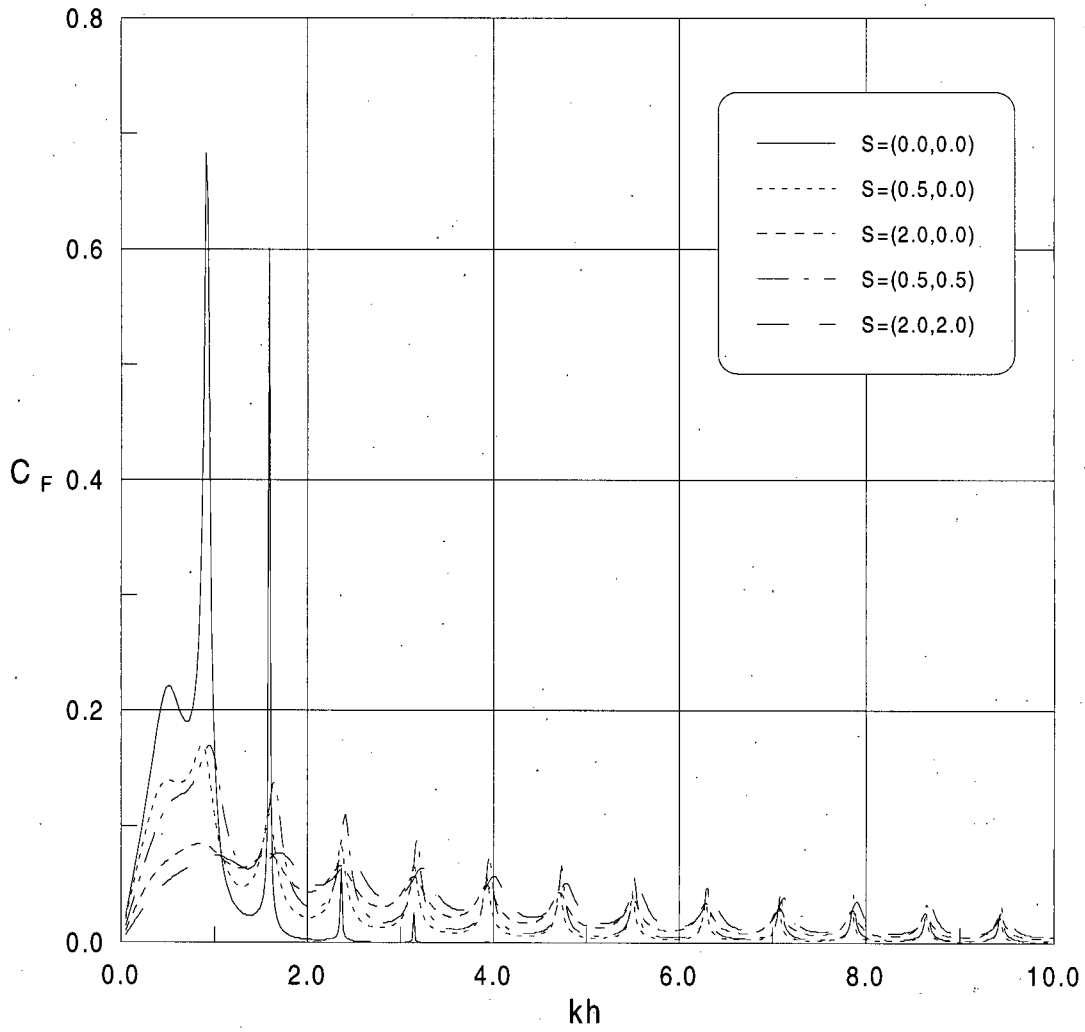

Figure 33 Force coefficient of the downwave barrier as a function of kh for $h/d = 0.5$, $\lambda/d = 1.0$ and for various values of S (two-barrier problem).

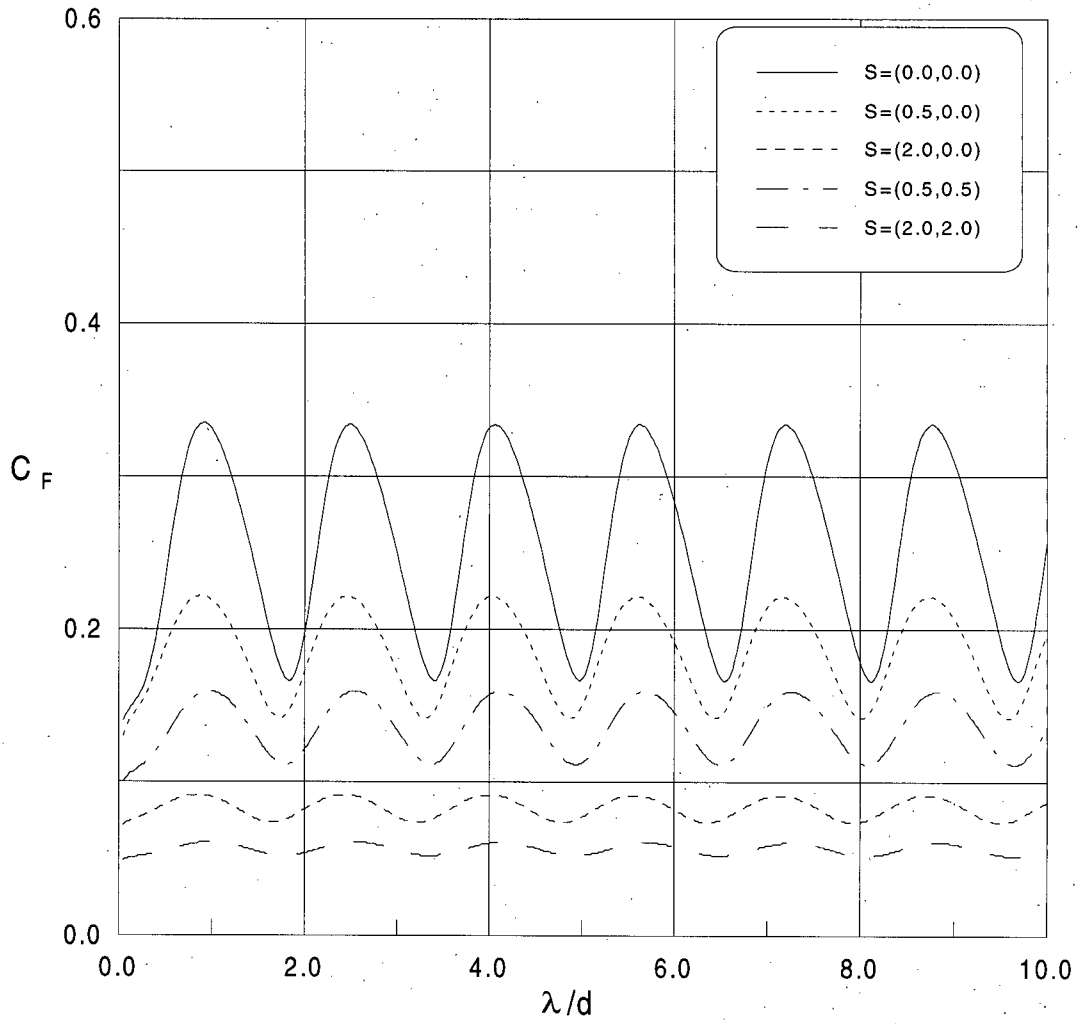

Figure 34 Force coefficient of the upwave barrier as a function of λ/d for $h/d = 0.5$, $kd = 1.0$ and for various values of S (two-barrier problem).

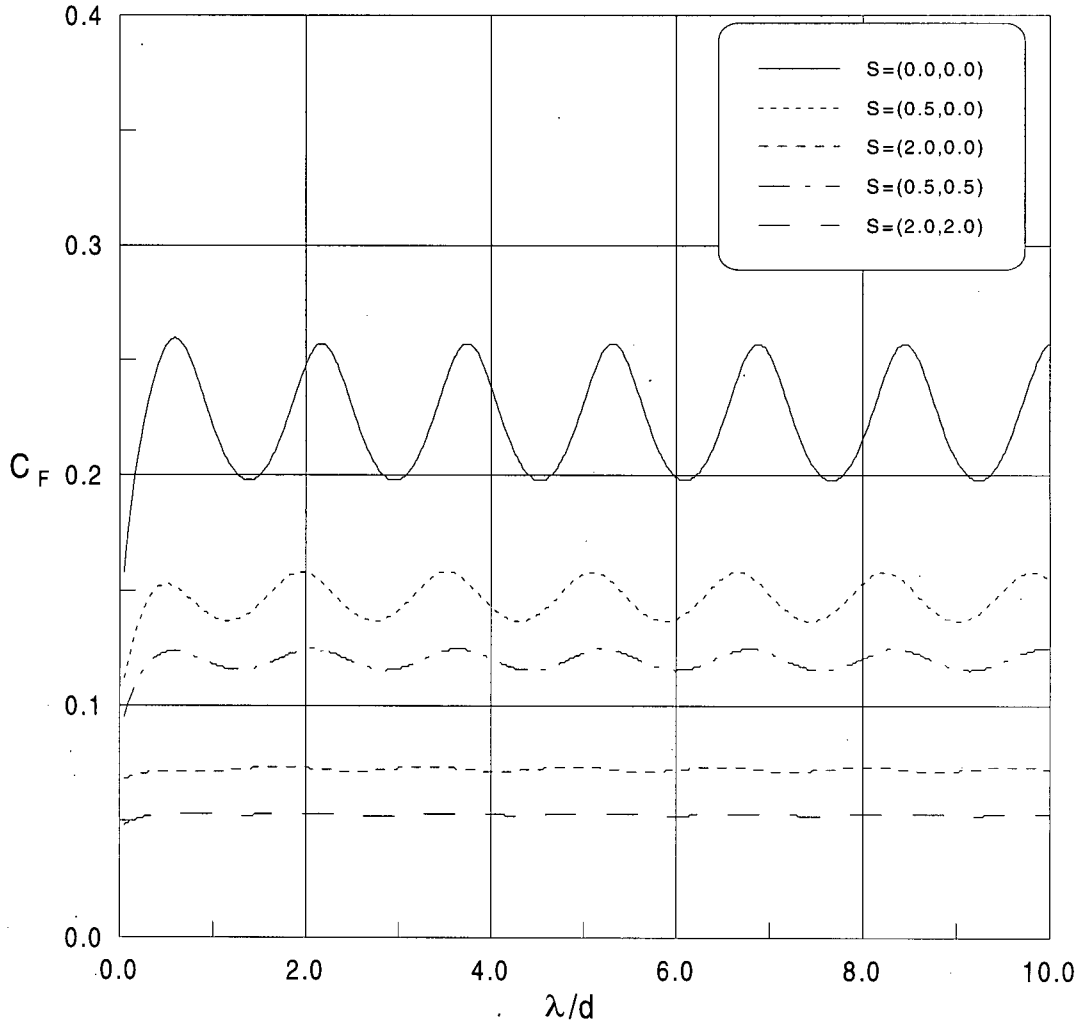

Figure 35 Force coefficients of the downwave barrier as function of λ/d for $h/d = 0.5$, $kd = 1.0$ and for various values of S (two-barrier problem).